

Instabilities of ablation fronts in inertial confinement fusion: A comparison with flames

P. Clavin^{a)}

Institut de Recherche sur les Phénomènes Hors Equilibre, Universités d'Aix Marseille et CNRS, 49 rue Joliot Curie, BP 146, 13384 Marseille Cedex 13, France

L. Masse

Commissariat à l'énergie atomique—Direction des applications militaires Île de France, BP 12, 91680 Bruyères le Châtel, France

(Received 11 August 2003; accepted 23 October 2003)

A comparison with flames sheds new light on the dynamics of ablation fronts in inertial confinement fusion (ICF). The mathematical formulation of the problem in ICF is the same as for flames propagating upwards. The difference concerns the Froude number F_r , yielding a different order of magnitude for the nondimensional wave number of the marginally stable disturbances. When the thermal conductivity varies strongly, as is the case in ICF, a wide range of characteristic (diffusive) lengths is involved across the wave structure. For disturbances with intermediate wavelengths, a “universal” diffusive relaxation rate of thermal waves is exhibited with no dependence on the heat conductivity. This is a key point for describing the dynamics of strongly accelerated ablation fronts whose marginally stable wavelength is much shorter than the total wave thickness. The coupling of hydrodynamics and heat conduction is analyzed in a way similar to flame theory, through the derivation of a kinematic relation for the ablation front including its thermal relaxation. A transition between the regimes of flames and ablation fronts in ICF is exhibited with decreasing F_r . For a moderate acceleration, $F_r \gg 1$, the result for flames is recovered. For a large acceleration, F_r of order unity, the thermal relaxation, when coupled with hydrodynamics, is shown to damp out the Darrieus–Landau instability, yielding the known result in ICF for strongly accelerated ablation fronts. For a wide class of models, including the simple two-length-scale model, the description is shown to be independent of the model. A weakly nonlinear analysis, valid irrespective of the number of unstable modes, is carried out for describing the early development of nonlinear structures of the ablation front in ICF. The role of the Darrieus–Landau instability at the early stage of irradiation is pointed out. © 2004 American Institute of Physics. [DOI: 10.1063/1.1634969]

I. INTRODUCTION

In inertial confinement fusion (ICF) the goal is to obtain high density and temperature for thermo-nuclear ignition near the center of the implosion of a spherical shell filled with a deuterium–tritium (DT) mixture.¹ In the direct-drive approach, mass ablation of the shell is produced by strong laser irradiation. The laser energy is absorbed at a critical surface, denoted by α_c , and located within the ablating plasma surrounding the shell at very high temperature, $T_c \sim 10^7 - 10^8$ K, $T_c \gg T_a$, and low density ρ_c , $\rho_c \ll \rho_a$, where subscript a refers to the cold dense region. The ablation velocity V_a of the material with density ρ_a is much smaller than the speed of sound and the approximation of low Mach number is valid, at least in the cold region. Due to large variations of the Spitzer thermal conductivity, $\lambda(T) = (T/T_a)^\nu \lambda_a$, $\nu \sim 5/2$, the diffusion length, $d = \lambda / \rho_a V_a C_p$, varies strongly across the plasma, from $d_a = \lambda_a / \rho_a V_a C_p$ in the cold region to d_c in the hot plasma, $d_a / d_c = (T_a / T_c)^\nu$, $d_a \ll d_c$. Pressure variations being negligible in first approximation, density varies like the inverse of temperature. However, in the limit $T_a / T_c \rightarrow 0$, the density variation is mainly

concentrated on the cold side in a small region where the ratio ρ / ρ_a varies from unity to a very small number, $\rho^* / \rho_a \ll 1$, on a distance d^* much smaller than the thickness of the total diffusion layer, $d_a < d^* \ll d_c$, see Fig. 1. The overall structure may then be approximated as a thermal conduction layer delimited by two free-boundaries, namely the critical surface $x = \alpha_c(y, t)$ and the ablation front $x = \alpha_a(y, t)$ across which the Atwood number $(\rho_a - \rho^*) / \rho_a$ is close to unity (x and y are the longitudinal and transverse coordinates, and t is the time).

The imploding shell is accelerated inward by the outside high pressure resulting from ablation, a phenomenon called “the rocket effect” in the literature. The ablation front is thus subject to a strong Rayleigh–Taylor (RT) instability. Degradation of spherical symmetry by hydrodynamic instabilities limits the achievable compression ratios and may prevent ignition. A considerable effort is currently underway to understand the hydrodynamic instability of ablation fronts in ICF.^{2–12} The linear growth rates of the corrugated front obtained by these analyses, exhibit a strong stabilization at small wavelength, due to mass ablation and called “dynamic overpressure” or “convective stabilization.” The physical reason for this stabilization is not obvious and not fully un-

^{a)}Electronic mail: clavin@irphe.univ-mrs.fr

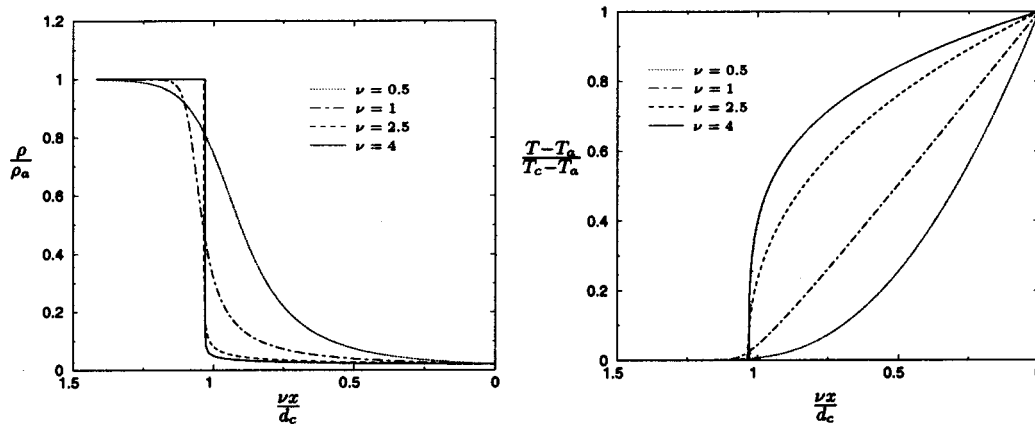


FIG. 1. Density and temperature profiles for a Spitzer type model with increasing ν and for $a = T_c/T_a = 50$.

derstood yet. An objective of this paper is to improve the physical insights, with a view of carrying out a nonlinear analysis. When attention is limited to the approximation of low Mach number, the formulation of the problem (equations and boundary conditions) is in fact the same as for flames propagating upwards, see Sec. II A below, but the order of magnitude of the dimensionless parameter for the acceleration g (inverse of the Froude number $F_r^{-1} \equiv g d_a / V_a^2$) is different. It is of interest to compare the different regimes, to see what implications our understanding of deflagrations may have for ICF ablation fronts. Surprisingly enough, the nature of the stabilization at small scales, looks quite different. Due to the Darrieus–Landau (DL) instability, flames are unstable to transverse disturbances, even for $g = 0$. The linear growth rate of this hydrodynamical instability is proportional to the product of the flame velocity with the wave number, $V_a k$, see Eq. (4) below. Every front propagating across a dense medium and transforming it into less dense products, is DL unstable to transverse disturbances whose wavelength is larger than the length-scale of density variation. This should be the case for ablation fronts in ICF for wavelengths larger than d^* . The well-known formula of Takabe *et al.*^{5,6} describes an opposite situation, see Eq. (1): A damping rate of the same form as the DL growth rate, with a change of sign, $-\beta V_a k$ and $\beta \approx 3$, competes with the RT instability whose growth rate is \sqrt{gk} . This damping rate is independent of the thermal conductivity, while that for flames is proportional to the product of the thermal diffusivity and the square of the wave number, $-D_T k^2$, corresponding to ordinary diffusive relaxation,^{13–15} see Eq. (6). How may a diffusive relaxation become independent of thermal diffusivity, and sufficiently strong to overcome the DL hydrodynamical instability, as is the case for ablation fronts in ICF? This question is addressed in the first part of the paper where the dynamics of ablation fronts is revisited with a method similar to the one used successfully in flame theory.^{13–16} The paper is self-contained, including background material which is recalled in Sec. II. In Sec. III, the problem is formulated in a general form, allowing coverage of the various regimes, from flames ($F_r^{-1} \ll 1$) to strongly accelerated ablation fronts in ICF (F_r^{-1} of order unity), and exhibiting for the first time the transition between these two regimes. Keeping in mind

that the final amplitude of the corrugations of the ablation front depends on an initial period of time (before the strong implosion) during which F_r^{-1} is negligible, such a general formulation is useful, not only from a fundamental point of view, but also for analyzing experiments or direct numerical simulations. The stabilization by transverse thermal conduction, occurring under the conditions of very strong RT instability, is explained in Sec. IV, within the framework of a “diffusive-thermal” model, free from hydrodynamical instability, by pointing out the conditions under which the relaxation rate of a pure (thermal) diffusion wave takes a universal “anti-DL” form, not depending on the thermal conductivity.

The coupling of hydrodynamics and thermal conduction is revisited in Secs. V and VI. Particular attention is paid to strong acceleration, such that the wavelengths of the unstable disturbances belong to an intermediate range, $d_* \ll 2\pi/k \ll d_c$. The linear stability has been previously analyzed either with a Spitzer conductivity in the limit $\nu \gg 1$, see Goncharov *et al.*,³ or within the framework of the so-called “sharp boundary model” (SBM) of Piriz *et al.*^{8,11} which was also used recently for nonlinear studies.¹² A crucial step with the SBM is the introduction of the so-called “self-consistent closure.” On the other hand, the problem was also solved analytically⁹ with a minimal model, called the “two-length-scale model,” in which the ablation front is considered as an isotherm, separating the overdense cool material and the blown-off plasma, with constant density and thermal conductivity on both sides. The solution of this ultra-simplified model is obtained without additional assumptions.⁹ In spite of a steady-state solution which differs from the Spitzer conductivity model, see Figs. 1 and 5, the linear and nonlinear analyses of the two-length-scale model^{9,17} yield the same results as those mentioned above.^{8,11,12} With a view to carrying out relevant analysis in the simplest way, general conditions of length-scale separation that are sufficient for making the results independent of the model, are presented in Sec. V A. A discontinuous model (with a discontinuity of heat conductivity at a temperature T_*) satisfying these conditions, and yielding a steady-state solution close to that for a continuous Spitzer conductivity is then introduced in Sec. V B. A noteworthy result is the systematic derivation of a

kinematic relation for the ablation front, see Eqs. (71) and (73), playing the same role as the self-consistent closure in the SBM, and describing the local modifications to the normal propagation velocity, due to thermal relaxation. In the limit $kd_c \gg 1$, as is the case for the most unstable disturbances of a strongly accelerated front (F_r of order unity), the kinematic relation takes a “universal” form, independent of the model: The ablation front is convected by the perturbed flow (more precisely by its value at the front) with a relaxation described by the “diffusive-thermal” model studied in Sec. IV, see Eqs. (71) and (73). Since the leading order of the flow is modified upstream and downstream of the ablation front, on a distance of the order of the wavelength, its local value at the front is well defined under the condition $kd_* \ll 1$. An equation for the overall dynamics of the ablation front is then obtained when the external flow is expressed as a functional of the corrugated ablation front, by solving the Euler equations with the boundary conditions at the ablation front, including the kinematic relation. This method not only greatly simplifies the analysis, but also improves physical insights and yields an appropriate framework for nonlinear studies.

The dispersion relation of Goncharov *et al.*³ corresponds to the choice T_* (and thus ρ_*) for which $kd(T_*) \approx 1$, as is expected for recovering the results for a continuous Spitzer conductivity by using a discontinuous model with two adjacent layers where $kd(T) \ll 1$ and $kd(T) \gg 1$, respectively. A preliminary study of the nonlinear dynamics is presented in Sec. VII where a weakly nonlinear pseudo-differential equation is derived for the evolution of the ablation front, valid without limit of the number of unstable modes, as for flames¹⁸ and detonations,¹⁹ but with the difference that, due to the RT instability, its validity is limited in time. The goal is different from recent analyses,^{12,17} and the motivation is here to address the two following problems. The first one concerns the formation of nonlinear structures, and their feeding mechanism. The disturbances that are the most linearly amplified during the final period of irradiation when the acceleration is strong (F_r^{-1} of order unity), have a wavelength much shorter than d_c , and thus, are strongly damped during the first period of irradiation, when the acceleration is negligible ($F_r^{-1} \ll 1$), see Fig. 2. An open question is whether or not these structures may be fed by a nonlinear transfer from initial disturbances with wavelengths, of order d_c or larger, that have been amplified by the DL instability during the first period ($F_r^{-1} \ll 1$). Another open question is whether or not “Huygens cusps” are formed by the normal propagation velocity of the front, as is the case for flames¹⁸ and detonations.¹⁹ In the weakly nonlinear study, particular attention is paid to the drastic simplification of potential flow, valid for strongly RT unstable ablation fronts, in the limit of large density jump, as noticed by Sanz *et al.*¹² The comparison with flames is once again amazing: For $g \approx 0$, a potential approximation is valid for the burned gas flow in the opposite limit of small density jump.²⁰ The form of the kinematic relation is the key point for explaining the difference.

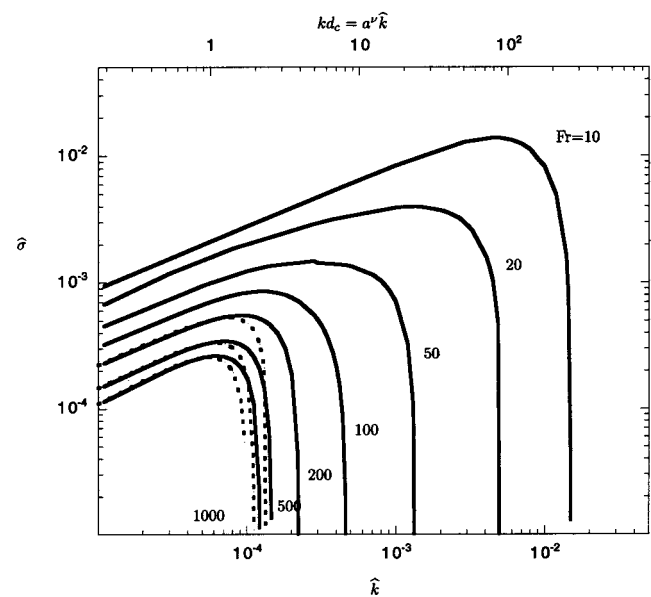


FIG. 2. Unstable spectrum. Numerical result (solid lines) for $a=50$ and for different Froude numbers ranging from 10 to 1000. The comparison shows a good agreement with the Clavin–Garcia result [dashed lines, see Eq. (8)] for $Fr > 350$ ($a^{\nu-1} Fr^{-1} < 1$) and with both the Goncharov *et al.* result (Ref. 3) and the numerical results of Kull (Ref. 7) for $Fr < 200$.

II. BACKGROUND, OPEN QUESTIONS, AND PHYSICAL INSIGHTS

A. Similarities and differences

In the limit of a large activation energy, the study of the dynamics of flame fronts was extended twenty years ago to a temperature-dependent thermal conductivity and a Lewis number close to unity.¹⁶ The exothermic reaction is confined to a thin layer on the hot side of the preheated zone of the flame structure ($T \sim T_c$), much thinner than the total flame thickness d_c (across which the temperature varies from T_a to T_c). By extending the Zel’dovich–Frank–Kamenetskii approach to wrinkled flames, see review papers,^{13–15} the reaction layer is considered as an hydrodynamic discontinuity, equivalent to the critical surface in direct drive.⁹ In flames, T_c is the adiabatic flame temperature, given by an energy balance, $C_p(T_c - T_a) = Q$, where Q is the chemical heat-release and C_p the specific heat, while for a direct-drive isobaric ablation front in ICF, the critical temperature T_c is given by the laser absorption (ρ_c corresponding to the plasma frequency at which the radiation is absorbed). The flame velocity V_a depends on the thermal conductivity, $\lambda(T_c)$ and on the reaction rate, both taken at T_c (high temperature). On the other hand, under the quasi-isobaric approximation, the ablation velocity V_a in ICF is fully determined by the laser intensity I and by $C_p(T_c - T_a)$, independently of the thermal conductivity, see Eq. (17). For flames and ablation fronts, the energy is transferred from the hot side to the cold region by thermal conduction. For a wrinkled flame with a unity Lewis number, the heat-conduction flux leaving the reaction layer is fully determined by the adiabatic flame temperature T_c , while the heat-conduction flux leaving the critical surface toward the ablation front is determined by the laser intensity. In both cases,

this flux is fixed. For a Spitzer conductivity, $\lambda = (T/T_a)^\nu \lambda_a$, $\nu > 1$, in the limit $T_a/T_c \rightarrow 0$, a sharp transition layer of temperature gradient, equivalent to the ablation front in ICF, also appears (for the same reason) on the cold side of the preheated zone of flames. The formulation of the problem is thus the same for flames and ablation fronts, as presented in Sec. III. In conclusion, the results for flames,¹⁶ which are valid for a moderate acceleration, $F_r^{-1} \ll (\rho_c/\rho_a)^{\nu-1}$, see Eqs. (7) and (8) below, must be also valid for ablation fronts in ICF at the early stage of irradiation, before implosion.

This is no longer the case for a strong acceleration, as shown by the formula of Takabe *et al.*,^{5,6} obtained by numerical fittings for the linear growth rate of an unstable transverse disturbance

$$\sigma \approx 0.9\sqrt{gk} - \beta V_a k, \tag{1}$$

where $\beta \approx 3$, and k is the modulus of the wave-number vector. The first term in the right hand side is the RT growth rate for an Atwood number close to unity, and the second describes a damping rate due to mass ablation. This phenomenology is confirmed by the leading order of the analytical result of Goncharov *et al.*³ obtained in the limit $\nu \gg 1$

$$\sigma \approx +\sqrt{kg - (\rho_a/\rho^*)(V_a k)^2} - 2V_a k, \tag{2}$$

where the density ratio ρ_a/ρ^* is large and depends on the wave number

$$(\rho_a/\rho^*) = \left(\frac{\nu}{kd_a}\right)^{1/\nu} \gg 1. \tag{3}$$

Equation (2) is written here at the leading order in the limit of Eq. (3), and is valid for conditions corresponding to a cut-off wave number lying in an intermediate range, $1/d_c \ll k \ll 1/d_a$. In the unstable range of Eq. (2), stabilization at small wavelength is due to the second term under the square root. In the limit $(\rho_a/\rho^*) \gg 1$, the last term in the right hand side of Eq. (2), $-2V_a k$, is a smaller stabilizing term, called ‘‘convective stabilization’’ in the ICF literature, describing the relaxation rate in the stable range (when the square root becomes imaginary).

The damping terms of ablation fronts in Eqs. (1) and (2) are surprising at first sight. An isobaric front propagating with a constant normal velocity V_a into a fluid of density ρ_a by transforming it into a less dense fluid, $\rho_c < \rho_a$, is known, since the work of Darrieus (1938) and Landau (1944), to be DL unstable with a linear growth rate

$$\sigma \approx +\sqrt{(\rho_a/\rho_c)V_a k}, \tag{4}$$

where the coefficient $\sqrt{(\rho_a/\rho_c)}$ is written here for simplicity in the limit of large density jump, $\rho_a/\rho_c \gg 1$ (the complete expression for this coefficient vanishes when $\rho_a = \rho_c$ and becomes negative when $\rho_a < \rho_c$). Equation (4) is obtained by considering the front as an hydrodynamic discontinuity (no reference length-scale in the model), and is valid only for disturbances whose wavelength, $2\pi/k$, is larger than the thickness of density variation. Under the same conditions and when the front is accelerated, one gets

$$\sigma \approx +\sqrt{kg + (\rho_a/\rho_c)(V_a k)^2} - V_a k + \dots, \tag{5}$$

where g is positive when the acceleration of the front is oriented toward the dense region. Notice that the RT instability ($g > 0$) of disturbances with a sufficiently small wavelength, $k > (\rho_c/\rho_a)g/V_a^2$, is dominated in Eq. (5) by the DL instability. The difference between Eqs. (2) and (5) is striking: Due to a change of sign, the term describing the small-wavelength instability in Eq. (5) (second term under the square root) is replaced in Eq. (2) by a stabilizing term of the same form. However, a full comparison cannot be completed without taking into account the diffusive stabilization at small wavelengths in Eq. (5).

B. Diffusive stabilization for moderate acceleration (the case of flames)

The stabilization of disturbances with small wavelength is due to thermal conduction in the transverse direction. An instructive example is provided by a purely reaction-diffusion wave (constant density, no hydrodynamic RT-DL instability) propagating at a constant velocity V_a , with a constant heat conductivity, $\lambda/\rho V_a C_p = Ct$, $d_a = d_c = d$. Such a reaction-diffusion wave involves only one length scale, d , and is stable with a damping rate corresponding to the classical diffusive relaxation

$$\sigma = -(\lambda/\rho C_p)k^2 = -(V_a d)k^2, \quad \forall kd, \tag{6}$$

valid at any wavelength $2\pi/k$.

Flame theory of the early 1980’s was devoted to describe the coupling of the diffusive relaxation in Eq. (6) with the DL hydrodynamic instability in Eq. (5) by using a perturbation analysis in the large wavelength limit,^{16,21-24} $kd_c \ll 1$. When a flame with a Spitzer thermal conductivity and a unity Lewis number is subjected to a constant and moderate acceleration (earth gravity, for example), the linear growth rate, $\sigma(k)$, is given by a root of the following quadratic equation,¹⁶ obtained at the first nontrivial order in the perturbation analysis, $kd_c \ll 1$:

$$\sigma^2 + 2\left(1 + \frac{kd_c}{\nu}\right)(V_a k)\sigma - kg - \frac{\rho_a}{\rho_c}(V_a k)^2\left[1 - \frac{2\nu + 1}{\nu(\nu + 1)}(kd_c)\right] = 0, \tag{7}$$

where the coefficients are written for simplicity at the leading order in the limit $\rho_a/\rho_c \gg 1$. In this limit, the leading order of the linear growth rate is

$$\sigma \approx +\sqrt{kg + (\rho_a/\rho_c)(V_a k)^2\left[1 - \frac{2\nu + 1}{\nu(\nu + 1)}(kd_c)\right]} - V_a k + \dots. \tag{8}$$

Equation (7) was obtained for studying the stability limits of flames propagating downward ($g < 0$, RT stable)¹⁶ and is also meaningful for $g > 0$ provided $kd_c \ll 1$. The pure hydrodynamic RT-DL instabilities in Eq. (5) are recovered by setting $kd_c = 0$ in Eqs. (7) and (8). The last term on the right-hand side of Eq. (8), $-V_a k$, is smaller, of relative order $\sqrt{\rho_c/\rho_a} \ll 1$, and can never overcome the DL instability which is represented by the second term under the square root. This $-V_a k$ term is of an hydrodynamic origin, and becomes use-

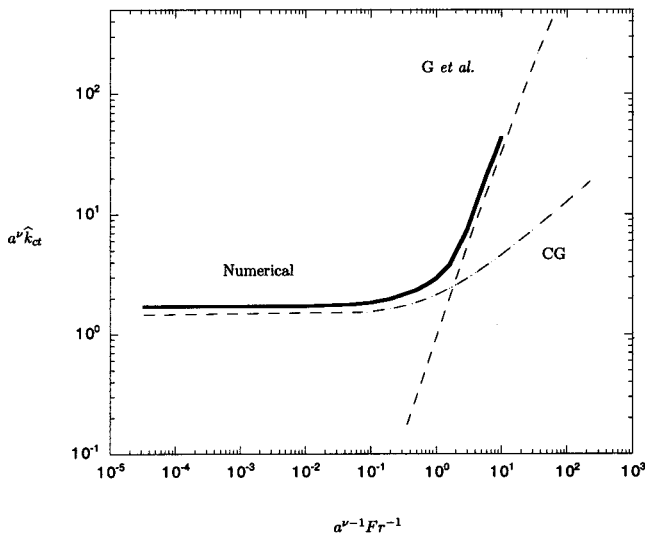


FIG. 3. Cut-off wave number ($a^\nu k_{ct}$) versus $(a^{\nu-1} Fr^{-1})$. Comparison of numerical results with the Clavin–Garcia result (CG), see Eqs. (7) and (8), and the Goncharov *et al.* result (G *et al.*), see Eq. (2), for $a=50$ and $\nu=5/2$.

ful in the stable domain, when the square root in Eq. (8) is imaginary. Notice the similarity with the last term in Eq. (2) but with a different coefficient. The stabilizing term, counteracting the RT and DL instabilities is the diffusive term proportional to $-kd_c$ inside the brackets [] in Eqs. (7) and (8). The result takes a self explanatory form by setting $g=0$ in Eq. (8)

$$\sigma \approx + \sqrt{(\rho_a/\rho_c)} \left[1 - \frac{2\nu+1}{2\nu(\nu+1)} (kd_c) \right] V_a k, \quad (9)$$

exhibiting a correction to the DL growth rate (4), due to a local change of the normal propagation velocity, $V_n \neq V_a$, induced by a relaxation mechanism, similar to the one in Eq. (6). As shown for self consistency, by recalling that the analysis is valid for kd_c shorter than unity, Eq. (8) describes accurately the full unstable range for moderate (RT unstable) acceleration, $gd_c/V_a^2 < \rho_a/\rho_c$, $Fr^{-1} < (\rho_c/\rho_a)^{\nu-1} \ll 1$. Equations (2) and (8) describe two different regimes, corresponding to different orders of magnitude for Fr . For moderate acceleration, $Fr^{-1} \approx (\rho_c/\rho_a)^{\nu-1}$ or smaller, the marginally stable wave number predicted by Eqs. (7)–(9) is of order $1/d_c$, indicating that the front becomes linearly stable for disturbances with wavelenth of the same order as the total thickness, or smaller. This is no longer true when the acceleration increases: According to Eq. (2), the marginally stable wave number is of order $g/(\rho_a/\rho^*)V_a^2$, corresponding to a wavelength much smaller than d_c , $kd_c \gg 1$, for strongly RT unstable ablation fronts, $gd_c/V_a^2 \gg \rho_a/\rho^*$, i.e., $Fr^{-1} \gg (\rho^*/\rho_a)^{\nu-1}$. The condition $Fr^{-1} > (\rho_c/\rho_a)^{\nu-1}$ is in fact the condition of validity of Eq. (2), see Fig. 3.

C. Universal relaxation rate for intermediate wavelengths (the case of strongly RT unstable fronts in ICF)

Under ordinary conditions of ICF, $kd^* \ll 1$, stabilization in Eqs. (1) and (2) cannot come from modifications to the

inner structure of the corrugated ablation front (of thickness d^*) because, according to Eqs. (8) and (9) when d_c is replaced by d^* , this would have introduced a diffusive correction of order $(\sqrt{\rho_a/\rho^*})(V_a d^*)k^2$. The transverse perturbations across the quasi-planar ablation front are negligible. Stabilization results from the transverse perturbations to the heat flux, downstream of the ablation front, across the thick thermal layer (between the ablation front and the critical surface). How is it possible that this diffusive damping may be independent of the thermal conductivity? Under what conditions, the whole phenomenon may be described as in the instability studies of the ablation front in ICF,^{2–8,10–12} without taking into account the corrugations of the critical surface which is the source of thermal energy? The answer is given in Secs. V and VI: The existence of a wide range of diffusion lengths $d(T)$, $d_a \ll d_c$, changes drastically the description, not only quantitatively but also qualitatively, as explained now, see Eqs. (6) and (10). A preliminary indication is provided in Sec. IV, by revisiting the relaxation of a purely thermal-wave (in the absence of hydrodynamical instability). For a diffusivity varying strongly across the wave structure, a transition appears in the relaxation mechanism: The damping rate of disturbances whose wavelengths are larger than d_c ($kd_c \ll 1$) has a form similar to the case involving a single diffusion length, see Eqs. (6) and (36), but in the opposite limit, for transverse disturbances whose wave numbers belong to an intermediate range, $1/d_c \ll k \ll 1/d_a$, the diffusive relaxation rate takes a quite different and universal form, not depending on the conductivity

$$\sigma \approx -V_a k. \quad (10)$$

From a physical point of view, Eq. (10) may be interpreted as the ordinary diffusive relaxation in Eq. (6), with a diffusivity taken at the location where the local diffusion length equals the wavelength, $kd(T)=1$. As shown in Sec. VI, see Eqs. (78) and (87), coupling hydrodynamics with diffusion shown in Eq. (10) will then lead to the “anti DL” stabilizing term described by the second term under the square root of Eq. (2), in a similar way as Eq. (8) results from the diffusive relaxation shown in Eq. (6).

III. QUASI-ISOBARIC MODEL

A. Formulation

Within a low Mach number approximation, $M^2 \ll 1$, $M^2 Fr^{-1} \ll 1$, density ρ , temperature T , flow velocity $\mathbf{v}=(u,v)$, and pressure p are described by the following set of equations:

$$\frac{D}{Dt} \rho + \rho \nabla \cdot \mathbf{v} = 0, \quad (11)$$

$$\rho \frac{D}{Dt} \mathbf{v} = -\nabla p + \rho \mathbf{g}, \quad (12)$$

$$\rho C_p \frac{D}{Dt} T = \nabla \cdot (\lambda \nabla T), \quad (13)$$

where \mathbf{g} is the acceleration of the wave, $D/Dt \equiv \partial/\partial t + (\mathbf{v} \cdot \nabla)$, and, according to the equation of state

$$\rho = \rho_a T_a / T. \tag{14}$$

Assuming that the laser radiation is absorbed at density ρ_c , the boundary conditions on the hot side is

$$x = \alpha_c: \quad T = T_c, \\ - (T_c / T_a)^\nu \lambda_a [\mathbf{n} \cdot \nabla T]_-^+ = I / \sqrt{1 + (\partial \alpha_c / \partial y)^2}, \tag{15}$$

$$x > \alpha_c: \quad \nabla T \approx 0, \quad \mathbf{v} \text{ bounded},$$

where \mathbf{n} an outward-pointing unit vector, normal to the critical surface, $x = \alpha_c(y, t)$, defined as the isotherm $T = T_c$. The boundary conditions in the cold fluid is

$$x \rightarrow -\infty: \quad T = T_a, \quad p = p_a, \quad \mathbf{v} = (V_a, 0), \tag{16}$$

where the flow velocity is written in the reference frame of the unperturbed wave (propagating relatively to the cold fluid at constant velocity, V_a).

The unperturbed solution is planar, $\mathbf{v} = (u, 0)$, $\rho u = \rho_a V_a$, and the problem reduces to that of solving a thermal equation (13). V_a is directly obtained by a spatial integration from $x = -\infty$ to the location of the critical condition, $T = T_c$, with the boundary conditions (15) and (16)

$$V_a = I / \rho_a C_p (T_c - T_a). \tag{17}$$

The distribution of temperature is given by the solution to Eq. (13). Integrating it from the cold side, $\bar{T}(\xi' = -\infty) = 1$, one gets

$$\bar{T}^\nu d\bar{T} / d\xi' = (\bar{T} - 1), \tag{18}$$

written in nondimensional form with the following notation:

$$\xi' = x / d_a, \quad \bar{T} = T / T_a, \quad a \equiv T_c / T_a = \rho_a / \rho_c.$$

Choosing the origin, $\xi' = 0$, at the critical surface, the temperature distribution is obtained by an integration of Eq. (18) with the boundary condition

$$\bar{T}(\xi' = 0) = a. \tag{19}$$

The boundary condition (15) is automatically satisfied, due to the choice of $d_a = \lambda_a / \rho_a V_a C_p$ where V_a is given by (17). The reduced solution $\bar{T}(\xi')$ depends only on the density ratio a and the exponent ν . For $a \gg 1$ and $\nu > 1$, and using the diffusion length at high temperature as reference length, $d_c = a^\nu d_a$, the solution exhibits a strong sharpness on the cold side, representative of the ablation front, where the main density jump is localized, see Fig. 1. When the cold side is used as reference for density, and the hot side as reference for temperature, see Fig. 1, the two distributions of density and temperature [linked by Eq. (14)] look very different. This illustrates the method used later in this paper where the hydrodynamic instability is approximated by using a density jump across the ablation front, while the diffusive relaxation is obtained by solving the temperature distribution for computing the heat flux coming from the critical surface by thermal conduction. Notice also that, according to (18), one has

$$\frac{\bar{T}^\nu}{\nu} \approx \xi' + \frac{a^\nu}{\nu}, \tag{20}$$

in the region where $\bar{T} \gg 1$.

For the study of unsteady and multidimensional cases, it is worth introducing the nondimensional mass flux in the normal direction across a given surface, $x = \alpha(y, t)$

$$m_\alpha \equiv \rho(u - \partial \alpha / \partial t - v \partial \alpha / \partial y) / \rho_a V_a \sqrt{1 + (\partial \alpha / \partial y)^2}, \tag{21}$$

and nondimensional coordinates in the moving frame, normalized by d_a and V_a / d_a

$$\xi = (x - \alpha(y, t)) / d_a, \tag{22}$$

$$\eta = y / d_a, \tag{23}$$

$$\tau = t V_a / d_a. \tag{24}$$

From now on, we use a splitting of each quantity in the form

$$X(\xi, \eta, \tau) = \bar{X}(\xi) + \tilde{X}(\xi, \eta, \tau),$$

where \bar{X} is the unperturbed value. The stability analysis of the steady state is performed using the linearized version of Eqs. (11)–(13) and Fourier decomposition

$$\tilde{\alpha} = \sum e^{+i\hat{k} \cdot \eta + \hat{\sigma} \tau} \hat{\alpha},$$

where the sum concerns the nondimensional wavevector \hat{k} . We also denote the modulus of the nondimensional wave vector, $|\hat{k}|$, and the complex nondimensional growth rate, respectively, as

$$\hat{k} \equiv k d_a, \quad \hat{\sigma} \equiv \sigma d_a / V_a,$$

and the Fourier decomposition of any field will be written as

$$\tilde{X}(\xi, \eta, \tau) = \sum e^{+i\hat{k} \cdot \eta + \hat{\sigma} \tau} \hat{X}(\xi) \frac{\hat{\alpha}}{d_a}.$$

With nondimensional variables

$$u / V_a \rightarrow u, \quad v / V_a \rightarrow v, \quad p / \rho_a V_a^2 \rightarrow p,$$

$$T / T_a \rightarrow T, \quad \rho / \rho_a \rightarrow \rho, \quad \alpha / d_a \rightarrow \alpha,$$

the linearized equations then become

$$\hat{\sigma} \hat{\rho} + d \hat{m}_\alpha / d \xi + \bar{\rho} i \hat{k} \hat{v} = 0, \tag{25}$$

$$\bar{\rho} \hat{\sigma} \hat{u} + d \hat{u} / d \xi + d \hat{p} / d \xi - \hat{\rho} F r^{-1} = - \hat{m}_\alpha d \bar{u} / d \xi, \tag{26}$$

$$\bar{\rho} \hat{\sigma} \hat{v} + d \hat{v} / d \xi + i \hat{k} \hat{p} = + i \hat{k} d \bar{v} / d \xi, \tag{27}$$

$$\bar{\rho} \hat{\sigma} \hat{T} + d \hat{T} / d \xi - d^2 (\bar{T}^\nu \hat{T}) / d \xi^2 + \hat{k}^2 \bar{T}^\nu \hat{T} \\ = - (\hat{m}_\alpha - \hat{k}^2 \bar{T}^\nu) d \bar{T} / d \xi, \tag{28}$$

with

$$F r^{-1} \equiv g d_a / V_a^2,$$

$$\hat{\rho} = - \bar{\rho} \hat{T} / \bar{T}, \quad \text{and} \quad \hat{m}_\alpha \equiv [\bar{u} \hat{\rho} + \bar{\rho} (\hat{u} - \hat{\sigma})].$$

B. Numerical stability results

As in flame theory, the problem is solved by using the critical surface in Eqs. (22)–(28)

$$\alpha = \alpha_c, \quad \xi = (x - \alpha_c) / d_a,$$

with the boundary conditions in Eqs. (15) and (16):

$$\xi \rightarrow -\infty: \quad \hat{\rho} = \hat{T} = \hat{u} = \hat{v} = 0, \tag{29}$$

$$\xi \geq 0: \quad \hat{T} = d\hat{T}/d\xi = 0, \tag{30}$$

$$\xi \rightarrow +\infty: \quad \hat{u} \quad \text{and} \quad \hat{v} \quad \text{bounded.}$$

For a given Froude number, Fr , the dispersion relation, $\hat{\sigma}(\hat{k})$, is obtained by solving numerically Eqs. (25)–(30) with the same shooting method as in flame theory. For a given \hat{k} , one starts from $\xi=0$ with two unknown constants (for the potential and rotational components of the flow), and one integrates toward the upstream conditions where the flow is potential and introduces a third unknown constant. Matching temperature \hat{T} and flow field $(\hat{u}, \hat{v}, \hat{\rho})$ yields $\hat{\sigma}$. The numerical results are plotted in Figs. 2 and 3, by comparison with the analytical results of Clavin–Garcia,¹⁶ see Eq. (7), and those of Goncharov *et al.*,³ see Eq. (2). For strong acceleration, $gd_c/V_a^2 \gg \rho_a/\rho_c$, $F_r^{-1} \gg 1/a^{\nu-1}$, the results are similar to the ICF results,^{3,5-7} obtained with a different boundary condition on the hot side, replacing Eq. (30) by

$$\xi \rightarrow +\infty: \quad \hat{T} = d\hat{T}/d\xi = 0.$$

This might be roughly explained by the fact that the temperature perturbation of unstable disturbances is localized on the ablation front and decreases toward zero with a length scale $1/k$, shorter than d_c . However, this argument should be taken with caution, as shown by the counter example of Sec. IV A below Eq. (37). For smaller accelerations, involved during the initial period of irradiation, $gd_c/V_a^2 \leq \rho_a/\rho_c$ (large Froude number $F_r \geq a^{\nu-1}$), the numerical solution to Eqs. (25)–(30) fits the Clavin–Garcia solution.¹⁶ The transition between the two regimes shown in Fig. 3 can be described only when the boundary condition (30) at the critical surface $\xi=0$ is used.

IV. DIFFUSIONAL-THERMAL RELAXATION

As in flame theory, it is instructive to study first the stabilization by thermal conduction, free from other effects (no hydrodynamics), within the framework of the so called “diffusional-thermal model,” defined by neglecting density fluctuations and flow perturbations in Eq. (13). This model reduces to an autonomous thermal equation (nonlinear Fourier equation)

$$\bar{\rho} \frac{\partial}{\partial \tau} T = \nabla \cdot (\lambda \nabla T), \tag{31}$$

written in the laboratory frame with nondimensional variables, $T/T_a \rightarrow T$, $\rho = 1/T$, $\tau = tV_a/d_a$, $\xi' = x/d_a$, $\eta' = y/d_a$ and $\lambda = T^\nu$ for a Spitzer conductivity. Solving Eq. (31) for $1 \leq T \leq T_c$ with boundary conditions (15) and (16)

$$T = T_c: \quad a^\nu \mathbf{n} \cdot \nabla T = 1/\sqrt{1 + (\partial \alpha_c / \partial y)^2}, \tag{32}$$

$$\xi' = -\infty: \quad T = 1,$$

one gets a free boundary problem for the critical surface $\xi' = \alpha_c(y, t)/d_a$, defined as the isotherm $T = T_c$. Its asymptotic solution for $\tau \rightarrow +\infty$ is the planar wave (18), propagating with a unity velocity. An interesting question, related to the stabi-

lization of corrugated ablation fronts, is the multidimensional stability of this diffusion wave. The corresponding linear equation, written in the moving frame of the critical surface, with the coordinates (22), $\xi = (x - \alpha_c)/d_a$, is obtained from Eq. (31)

$$\frac{d^2}{d\xi^2} (\bar{\lambda} \hat{T}) - \frac{d}{d\xi} \hat{T} - (\bar{\rho} \hat{\sigma} + \bar{\lambda} \hat{k}^2) \hat{T} = -(\bar{\rho} \hat{\sigma} + \bar{\lambda} \hat{k}^2) \frac{d}{d\xi} \bar{T}, \tag{33}$$

with

$$\bar{\lambda} = \bar{T}^\nu,$$

to be solved with the boundary conditions in Eqs. (29) and (30). Equation (33) corresponds to Eq. (28) by setting $\hat{\rho} = 0$ and $\hat{u} = 0$. An even simpler model, useful for describing the linear dynamics of a diffusive wave with a varying diffusivity, is obtained by setting $\bar{\rho} = 1$ (no density variation) in Eq. (33).

A. Solution for the Spitzer model

Within the framework of a continuous Spitzer conductivity, two limiting cases may be solved analytically, $kd_c (\equiv a^\nu \hat{k}) \ll 1$ and $kd_c \gg 1$. Consider first the case $kd_c \ll 1$ for $\bar{\rho} = 1$. When $a^\nu \hat{k} \ll 1$, $\hat{\sigma}$ and $\bar{\lambda} \hat{k}^2$ are small quantities of same order, and \hat{T} is also small, $\hat{T} = O(a^{\nu+1} \hat{k}^2)$, smaller than $d\bar{T}/d\xi = O(1/a^{\nu-1})$. The dominant order of Eq. (33) is

$$\frac{d}{d\xi} \hat{T} - \frac{d^2}{d\xi^2} (\bar{T}^\nu \hat{T}) \approx (\hat{\sigma} + \bar{T}^\nu \hat{k}^2) \frac{d}{d\xi} \bar{T}, \tag{34}$$

yielding, according to (30)

$$\int_1^a (\hat{\sigma} + \bar{T}^\nu \hat{k}^2) d\bar{T} = 0, \tag{35}$$

$$\Rightarrow \hat{\sigma} = -\frac{\hat{k}^2}{\nu+1} \frac{(a^{\nu+1}-1)}{(a-1)} \approx -\frac{a^\nu}{\nu+1} \hat{k}^2 \sigma$$

$$\approx -(V_a d_c) k^2 / (\nu+1),$$

with

$$\hat{T} = \frac{d\bar{T}}{d\xi} \left[\hat{\sigma} \xi - \frac{\hat{k}^2}{\nu+1} \int_0^\xi \left(\frac{\bar{T}^{\nu+1}-1}{\bar{T}-1} \right) d\xi' \right]. \tag{36}$$

Equation (36) is similar to the result in Eq. (6) but, limited here to $kd_c \ll 1$. A similar result is also obtained for variable density, $\bar{\rho} = 1/\bar{T}$

$$\hat{\sigma} = -\frac{\hat{k}^2}{\nu+1} \frac{(a^{\nu+1}-1)}{\ln a} \approx -\frac{(a^{\nu+1}/\ln a)}{\nu+1} \hat{k}^2. \tag{37}$$

Although the perturbed temperature is, according to Eq. (36), localized at the ablation front, see Fig. 4, the relaxation is controlled by the thermal conductivity at high temperature.

Let us consider now the intermediate case $1/d_c \ll k \ll 1/d_a$, ($1/a^\nu \ll \hat{k} \ll 1$). Introducing a new variable, $\hat{\phi} = \bar{T}^\nu (\hat{T} - d\bar{T}/d\xi)$, Eq. (33) with $\bar{\rho} = 1$ leads to

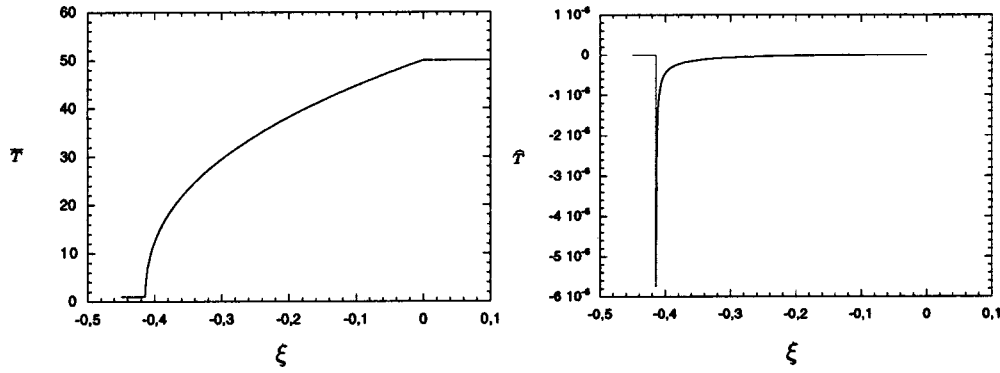


FIG. 4. Steady (left figure) and perturbed (right figure) temperature profiles, for $a=50$, $n=5/2$, and $kd_c=10^{-3}$.

$$\frac{d^2}{d\xi^2} \hat{\phi} - \frac{d}{d\xi} \left(\frac{\hat{\phi}}{\bar{T}^\nu} \right) - \left(\frac{\hat{\sigma}}{\bar{T}^\nu} + \hat{k}^2 \right) \hat{\phi} = 0, \tag{38}$$

to be solved with the boundary conditions (29) and (30), written as

$$\hat{\phi}(\xi = -\infty) = 0, \tag{39}$$

$$\hat{\phi}(\xi = 0) = -(a-1) \approx -a, \tag{40}$$

$$\left. \frac{d}{d\xi} \hat{\phi} \right|_{\xi=0} = -\frac{(a-1)}{a^\nu} \approx 0, \tag{41}$$

where the approximations are for $a \gg 1$. An approximated solution to this problem is obtained in the following manner. In the hot region where $\hat{k}\bar{T}^\nu \approx \hat{k}a^\nu \gg 1$, Eq. (38) reduces to Laplace equation

$$d^2 \hat{\phi} / d\xi^2 - \hat{k}^2 \hat{\phi} \approx 0,$$

and the leading order solution which satisfies the boundary conditions (40) and (41) on the hot side at $\xi=0$, is

$$\hat{\phi} \approx -\frac{1}{2}(a-1)[e^{+\hat{k}\xi} + e^{-\hat{k}\xi}], \tag{42}$$

valid when terms of order $1/a^{\nu-1}$ are neglected. When the constant a is replaced in Eq. (42) by $\bar{T}(\xi)$, one gets

$$\hat{\phi} \approx -\frac{1}{2}(\bar{T}-1)[e^{+\hat{k}\xi} + e^{-\hat{k}\xi}], \tag{43}$$

$$\hat{T} \approx -\frac{1}{2} \frac{d\bar{T}}{d\xi} [e^{+\hat{k}\xi} + e^{-\hat{k}\xi} - 2],$$

expressions which satisfy the upstream and downstream boundary conditions. When they are introduced in the left hand side of Eq. (38), one gets

$$\frac{1}{2} \frac{d\bar{T}}{d\xi} [(\hat{\sigma} + \hat{k})e^{-\hat{k}\xi} + (\hat{\sigma} - \hat{k})e^{+\hat{k}\xi}], \tag{44}$$

a quantity which becomes negligible close to the critical surface, where $d\bar{T}/d\xi$ is of order $1/a^{\nu-1}$. On the other hand, sufficiently far from the critical surface, $\xi \ll -1/\hat{k} < 0$, ($e^{+\hat{k}\xi} \ll 1$ and $e^{-\hat{k}\xi} \gg 1$), according to Eqs. (43), the perturbation of the temperature fields reduces to

$$\hat{T}(\xi) \approx -\frac{1}{2} \frac{d\bar{T}}{d\xi} e^{-\hat{k}\xi},$$

$$\bar{T} \approx -\frac{1}{2} \frac{d\bar{T}}{d\xi} \sum \left[(e^{+i\hat{k} \cdot \eta + \hat{\sigma}\eta}) \frac{\hat{\alpha}_c}{d_a} e^{-\hat{k}\xi} \right], \tag{45}$$

and the quantity in Eq. (44) also becomes negligible, provided that Eq. (10) is satisfied,

$$\hat{\sigma} = -\hat{k} \Rightarrow \sigma = -kV_a. \tag{46}$$

This shows that Eqs. (43) are approximate solutions to Eq. (38), fitting the exact ones on both sides (high and low temperature) and yielding, according to Eq. (46), a relaxation rate in the form of an anti DL stabilizing term, not depending on the thermal conductivity. Equations (36) and (46) indicate the existence of a transition in the relaxation rate which appears for thermal waves involving a large range of diffusion lengths. This transition may be described analytically with the simple model presented below.

B. Two-length-scale model

Equation (46) is in fact generic for intermediate wavelengths, $1/d_c \ll k \ll 1/d_a$, in the sense that it does not depend on how the thermal conductivity varies, as shown by the following model which may be solved without approximation. Consider Eq. (33) with a piecewise constant thermal conductivity and density, with a jump at a fixed temperature $T = T_*$

$$\begin{aligned} \lambda &= 1, & \bar{\rho} &= 1, & \forall T < T_*, \\ \lambda &= (d_c/d_a), & \bar{\rho} &= 1/a_*, & \forall T > T_*. \end{aligned} \tag{47}$$

Only two length scales are now introduced in the problem, d_a and d_c . The equation of the isotherm $T = T_*$ will be denoted $x = \alpha_a(\eta, \tau)$, $\alpha_a < 0$, $\bar{\alpha}_c = 0$. The density jump, $\rho_* = 1/T_* \neq 1$, does not play an essential role in the diffusional-thermal relaxation, but will be useful later, when dealing with hydrodynamic instabilities. The steady-state solution, written in dimensional variables, is, see Fig. 5

- $x < \bar{\alpha}_a$ (cold side): $\bar{T} = \bar{T}_-$
 $\bar{T}_- - T_a = (T_* - T_a)e^{(x - \bar{\alpha}_a)/d_a}$
- $\bar{\alpha}_a < x < 0$ (hot side) $\bar{T} = \bar{T}_+$:

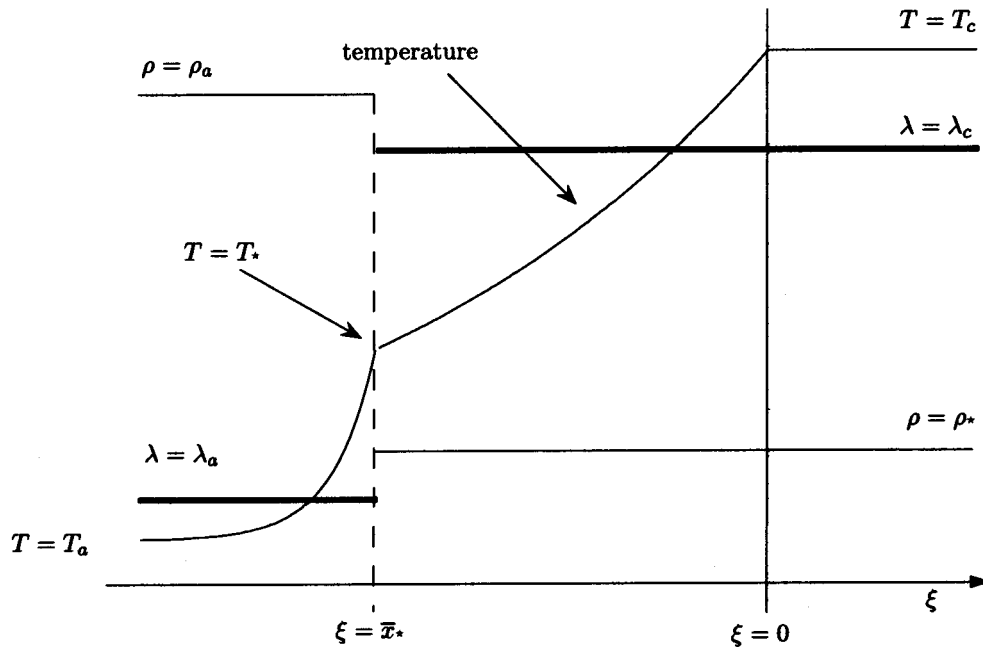


FIG. 5. Temperature and density profiles for the two-length-scale model.

$$\bar{T}_+ - T_a = (T_c - T_a)e^{x/d_c},$$

with

$$(T_* - T_a)/(T_c - T_a) = e^{\bar{\alpha}_a/d_c} < 1, \tag{48}$$

for insuring continuity of the heat flux at T_* . Equation (33) reduces to a second order ordinary differential equation (ODE) with constant coefficients and can be solved explicitly on both sides. Solutions to the homogeneous equation are written in the form, $e^{r_a^+ \xi}$, $\xi = (x - \alpha_a)/d_a$, in the cold side, $T < T_*$, and $e^{r_c^\pm \xi}$, $\xi = (x - \alpha_c)/d_a$, in the hot side, $T > T_*$, with

$$r_a^+ = \frac{1}{2} [1 + \sqrt{1 + 4(\hat{\sigma} + \hat{k}^2)}], \tag{49}$$

$$r_c^\pm = \frac{1}{2} \frac{d_a}{d_c} \left[1 \pm \sqrt{1 + 4 \left(\frac{1}{a_*} \frac{d_c}{d_a} \hat{\sigma} + \left(\frac{d_c}{d_a} \hat{k} \right)^2 \right)} \right]. \tag{50}$$

The computation of the temperature field is tedious but straightforward.⁹ The dispersion relation, $\sigma(k)$ is obtained by imposing continuity of heat flux at $T = T_*$ and the boundary conditions (29) at $\xi \rightarrow -\infty$ and (30) at $\xi = 0$. The result in Eq. (6) is recovered for $d_a = d_c = d$. In the case $d_a \ll d_c$, a transition, similar to the one observed in Fig. 3, is observed. The long wavelength limit yields a result similar to Eq. (36), with a different numerical coefficient. For disturbances with intermediate wavelengths, $kd_a \ll 1 \ll kd_c$, and when $|\bar{\alpha}_a|$ and d_c are of same order of magnitude, transcendental small terms, such as $e^{-k|\bar{\alpha}_a|}$, may be neglected, and the dispersion relation reduces to

$$r_a^+ - 1 \approx r_c^-, \tag{51}$$

expressing the continuity of heat flux at T_* , see the solutions for \bar{T} in Eqs. (54) and (56) below. Equation (51) leads to the dispersion relation (46), as can be seen from the following approximations

$$kd_c \equiv \hat{k}d_c/d_a \gg 1 \Rightarrow r_c^\pm \approx \pm \hat{k},$$

$$\hat{k} \equiv kd_a \ll 1 \Rightarrow r_a^+ \approx 1 + \hat{\sigma},$$

expressing that the evolution time scale for the ablation front is much longer than two other time scales, namely the transit time across the quasi-planar upstream layer (of thickness d_a , $\hat{k} \equiv kd_a \ll 1$), and the relaxation time toward a quasi-steady state approximation in the thermal layer (of thickness d_c) for the perturbed temperature which satisfies the Laplace equation in first approximation.

For further analysis in Sec. VIA, it is worth giving more details of the intermediate case $kd_a \ll 1 \ll kd_c$. The temperature field may be computed on the hot side ($T > T_*$) by using the boundary conditions at the critical surface (30) at $\xi = 0$. In a region sufficiently far from the critical surface, $\xi = (x - \alpha_c)/d_a \ll -1/\hat{k}$, where $e^{r_c^+ \xi} \ll 1$ and $e^{r_c^- \xi} \gg 1$, the perturbation of temperature takes the form

$$\begin{aligned} \tilde{T}_+(\xi) \approx & \frac{d\bar{T}_+}{d\xi} \frac{\tilde{\alpha}_c}{d_a} - \frac{(T_c - T_a)}{2(d_c/d_a)} \\ & \times \sum \left[(e^{+i\hat{k} \cdot \eta + \hat{\sigma}\tau}) \frac{\hat{\alpha}_c}{d_a} e^{r_c^- \xi} \right], \end{aligned} \tag{52}$$

where higher-order terms, $(d_a/d_c)^n$, $n > 1$, have been neglected in the coefficient of the second term on the right hand side. The ratio of the amplitudes of the corrugations of the two fronts (ablation and critical) is obtained from Eq. (52), by using the definitions of T_* and α_a

$$T_+|_{\xi=(\alpha_a-\alpha_c)/d_a}=\bar{T}|_{\xi=\bar{\alpha}_a/d_a}\equiv T_*, \tag{53}$$

with $T_+(\xi)=\bar{T}_+(\xi)+\tilde{T}_+(\xi)$ and $\bar{\alpha}_c=0$,

$$\Rightarrow \tilde{T}_+|_{\xi=\bar{\alpha}_a/d_a}=-\frac{(\tilde{\alpha}_a-\tilde{\alpha}_c)}{d_a}(d\bar{T}_+/d\xi)|_{\xi=\bar{\alpha}_a/d_a},$$

valid under the linear approximation, yielding in Fourier representation in the limit $k|\bar{\alpha}_a|\gg 1$

$$\frac{\hat{\alpha}_a}{\hat{\alpha}_c}\approx\frac{1}{2}\frac{(T_c-T_a)}{(T_*-T_a)}e^{r_c^-\bar{\alpha}_a/d_a}\gg 1,$$

where $\bar{\alpha}_a < 0$ and $r_c^- \approx -\hat{k}$. This result which is limited to small perturbations (linear approximation), shows how small is the amplitude of the corrugations of the critical surface compared to the ablation front. By noticing that, near the ablation front, the first term on the right hand side of Eq. (52) is negligible, and using the above equation to eliminate $\hat{\alpha}_c$, the perturbation of temperature in the hot side may be expressed in term of the corrugations of the ablation front

$$\begin{aligned} \tilde{T}_+ &\approx -(d\bar{T}_+/d\xi)|_{\xi=\bar{\alpha}_a/d_a} \\ &\times \sum \left[(e^{+i\hat{k}\cdot\eta+\hat{\sigma}\tau}) \frac{\hat{\alpha}_a}{d_a} e^{-k(x-\bar{\alpha}_a)} \right]. \end{aligned} \tag{54}$$

This result shows that the perturbation of the temperature satisfies a Laplace equation with a zero boundary value at $x \rightarrow +\infty$, and a boundary value at the ablation front, simply given by the shift of the isotherm T_* . A similar result is obtained with a Spitzer model from Eq. (45) for the isotherm $T=T^*$, $x=\alpha_a(\eta, \tau)$

$$\hat{\alpha}_a/\hat{\alpha}_c \approx (1/2)e^{-k\bar{\alpha}_a} \gg 1, \tag{55}$$

$$\tilde{T}_+(\xi) \approx -\frac{d\bar{T}}{d\xi}(\xi) \sum \left[(e^{+i\hat{k}\cdot\eta+\hat{\sigma}\tau}) \frac{\hat{\alpha}_a}{d_a} e^{-k(x-\bar{\alpha}_a)} \right].$$

The distribution of the perturbation of temperature in Eqs. (54) and (55) is strongly peaked around $x=\bar{\alpha}_a$ as in Fig. 4. Coming back to the two-length-scale model, the perturbation of temperature on the cold side, $T < T^*$, is easily computed in the moving frame of the isotherm $T=T_*$, using the variable $\zeta=(x-\alpha_a)/d_a$,

$$\begin{aligned} \tilde{T}_-(\xi) &\approx \frac{d\bar{T}_-}{d\zeta} \frac{\tilde{\alpha}_a}{d_a} - (d\bar{T}_-/d\zeta)|_{\zeta=0} \\ &\times \sum \left[(e^{+i\hat{k}\cdot\eta+\hat{\sigma}\tau}) \frac{\hat{\alpha}_a}{d_a} e^{r_a^+\zeta} \right]. \end{aligned} \tag{56}$$

Continuity of the heat flux at $T=T_*$, $x=\alpha_a$, computed from Eqs. (54) and (56), yields the result (51) and leads to the dispersion relation (46), valid for an intermediate range of wavelengths, independently of the precise choice of T_* , showing that the simple model (47) is sufficient to reproduce the universal relaxation rate (10).

V. THE COUPLING OF HEAT TRANSFER AND HYDRODYNAMICS FOR INTERMEDIATE WAVELENGTHS, $1/d_c \ll k \ll 1/d_*$

The coupling of thermal conduction and fluid mechanics, governing the linear dynamics of strongly RT unstable ablation front, may be solved analytically within the framework of the two-length-scale model (47), without approximation.⁹ General approximations that are useful for carrying out analytical solutions to more general models in the intermediate range of wavelengths $1/d_c \ll k \ll 1/d_*$, may be extracted from this analysis. These conditions are presented below; they define a class of models yielding universal results (independent of the model). A more realistic model than (47) is then presented, see Eq. (65), and the results are obtained in Secs. VI and VII, following a method similar to the one used in flame theory.^{13-16,24}

A. Basic approximations

When attention is limited to disturbances whose wavelengths are larger than the thickness of the ablation front, $kd_* \ll 1$, this thin layer is quasi-planar and quasi-steady in first approximation, and may be considered as a hydrodynamical discontinuity. Its perturbed propagation velocity, relative to the cold (upstream) flow, may be computed as in flame theory by a multiple-scale method.^{13-16,24} At the leading order, the calculation is similar to that for the steady state solution, the external heat flux (due to thermal conduction downstream the ablation front) playing the same role as the laser intensity in the computation of the velocity of an unperturbed thermal wave, see Eqs. (15) and (17) compared to Eq. (59). Using coordinates defined in Eq. (22), but now relative to the moving frame of the ablation front

$$\alpha = \alpha_a,$$

we introduce the mass flux m_a crossing the surface $x = \alpha_a(y, t)$, defined in Eq. (21) (when α is replaced by α_a). Mass conservation (11) shows that the leading order of m_a is constant across the ablation front²⁴

$$m_a = \frac{(u_{a-} - \partial\alpha_a/\partial t - v_{a-}\partial\alpha_a/\partial y)}{V_a\sqrt{1+(\partial\alpha_a/\partial y)^2}}, \tag{57}$$

$$= \left(\frac{\rho_*}{\rho_a}\right) \frac{(u_{a+} - \partial\alpha_a/\partial t - v_{a+}\partial\alpha_a/\partial y)}{V_a\sqrt{1+(\partial\alpha_a/\partial y)^2}}, \tag{58}$$

where ρ_* is the density at the downstream exit of the ablation layer, and $(u_{a\pm}, v_{a\pm}) \equiv (u_{\pm}, v_{\pm})_{x=\alpha_a}$ are the values of the components of the downstream and upstream flow velocity, taken at the ablation front. These last quantities are well defined at the leading order of the multiple-scale analysis for $kd_* \ll 1$, because the characteristic length-scale of the external flow is $(2\pi/k)$, see Eqs. (79)–(82), larger than the thickness of the ablation front d_* . Under quasi-planar and quasi-steady approximations, the integration of the conservation of energy (13) across the ablation front leads to an equation similar to (18)

$$\left(\frac{T}{T_a} - 1\right) m_a = d_a \lambda \frac{d}{d\zeta_n} \left(\frac{T}{T_a}\right),$$

where ζ_n is the coordinate in the direction normal to the isotherms, and $\lambda \equiv (T/T_a)^\nu$ for the Spitzer model. Matching temperature and heat flux at the exit of the ablation front with the “external” solution on the hot side, leads to a relation similar to Eqs. (15) and (17)

$$\left(\frac{T_*}{T_a} - 1\right) m_a = d_a \left[\lambda \mathbf{n} \cdot \nabla \left(\frac{T_+}{T_a} \right) \right]_{x=\alpha_a}, \quad (59)$$

where $x = \alpha_a(y, t)$ is the isotherm $T_+(x, y, t) = T_*$. In the same approximation, the flow satisfies the following jumps across the ablation front:²⁴

$$\frac{v_{a-} - v_{a+}}{V_a} = \left(\frac{\rho_a}{\rho_*} - 1 \right) m_a \frac{\partial \alpha_a / \partial y}{\sqrt{1 + (\partial \alpha_a / \partial y)^2}}, \quad (60)$$

$$\frac{p_{a-} - p_{a+}}{\rho_a V_a^2} = \left(\frac{\rho_a}{\rho_*} - 1 \right) m_a^2, \quad (61)$$

expressing the conservation of momentum, subscripts \pm identifying conditions downstream and upstream from the ablation front. As in flame theory, curvature effects may be easily taken into account by pushing the perturbative analysis to the following orders of the power expansion in kd_* . This refinement is not necessary in the analysis of Secs. VI and VII.

The temperature variations in the thermal conduction zone, downstream from the ablation front, necessary to compute the right-hand side of Eq. (59), are obtained from Eq. (13). In the region where the relation $kd(T) \gg 1$ holds, hydrodynamic and unsteady effects are small compared to advection and thermal conduction, and Eq. (13) reduces to the steady version of the diffusional-thermal model

$$\frac{\partial T_+}{\partial \xi'} = \nabla \cdot [\lambda(T_+) \nabla T_+], \quad (62)$$

written here in nondimensional form, $T/T_a \rightarrow T$, and in the reference frame of the unperturbed wave, $\xi' = x/d_a$, $\eta' = y/d_a$. For a Spitzer conductivity, one gets

$$\frac{\partial T_+}{\partial \xi'} = \left(\frac{\partial^2}{\partial \xi'^2} + \frac{\partial^2}{\partial \eta'^2} \right) \frac{T_+^{\nu+1}}{\nu+1}.$$

Introducing the splitting

$$\frac{T_+^{\nu+1}}{\nu+1} \equiv \frac{\tilde{T}_+^{\nu+1}}{\nu+1} + \tilde{Z},$$

the leading order of \tilde{Z} satisfies a Laplace equation. Even for finite amplitude of the corrugations of the ablation front, $\tilde{Z}(\xi)$ may be computed by using the linearized boundary conditions at the critical surface, where the temperature disturbances are very small. In the region where $kd(T) \gg 1$, each isotherm is fully determined in term of the critical surface $x = \alpha_c(y, t)$ by solving Eq. (62) with (15). This is also the case of the ablation front, $x = \alpha_a(y, t)$, if the isotherm $T = T_*$ belongs to this region, or at least to a boundary layer adjacent to this region. For computing the flow field, the density profile in Fig. 1 suggests that the hydrodynamic effects may be approximated by taking into account only the

density variations across the thin ablation front, the density in Eqs. (11) and (12) being considered as constant in the external regions. More precisely, downstream from the ablation front, the nondimensional flow is proportional to a large number, ρ_a/ρ_* , and varies on a length scale proportional to the wavelength, $2\pi/k$, see Eq. (95), while density variations are of order unity, $\Delta\rho/\rho_* = O(1)$, and involves a longer length scale, the diffusion length d . The hydrodynamic effects associated with the density variations in the region of the conduction layer where $kd \gg 1$, are small and may be neglected, and, according to Eqs. (11) and (12), the flow is solution to

$$\nabla \cdot \tilde{\mathbf{v}}_{\pm} = 0, \quad (63)$$

$$\bar{\rho}_{\pm} \frac{D}{Dt} \mathbf{v}_{\pm} = -\nabla p_{\pm} + \bar{\rho}_{\pm} \mathbf{g}, \quad (64)$$

where $\bar{\rho}_{\pm}$ are considered as constant quantities in first approximation, $\bar{\rho}_- = \rho_a$ and $\bar{\rho}_+$ is a slowly varying quantity from ρ_* to ρ_c , involving length scales of order $d(T)$.

B. Model and method

For a continuous Spitzer conductivity, there is always an intermediate layer where kd is of order unity, $\hat{k}\bar{T}^\nu = O(1)$, and where none of the simplifications (57)–(64) are valid. Solving analytically this transition region where the different effects are all of the same order of magnitude, is beyond our capacity, even in the linear approximation. The difficulty may be bypassed by considering models in which the thermal conductivity (and the diffusive length) is discontinuous at a temperature T_* (T_* defining the position of the ablation front), such that both conditions $kd(T) \ll 1$, $\forall T < T_*$, and $kd(T) \gg 1$, $\forall T > T_*$, hold. Among these models, the one which is the closest to a continuous Spitzer conductivity is

$$\lambda = \begin{cases} \lambda_-(T), & \forall T < T_*, \\ \lambda_+(T) = (T/T_a)^\nu \lambda_a, & \forall T > T_*, \end{cases} \quad (65)$$

where $\lambda_-(T)$ is increasing with T , from $\lambda_-(T_a) = \lambda_a$ to $\lambda_-(T_*)$ with $\lambda_-(T_*) \ll (T_*/T_a)^\nu \lambda_a$. The length $d_-(T_*) \equiv \lambda_-(T_*)/\rho_a V_a C_p$ represents the thickness of the ablation front ($T_a < T < T_*$), and is denoted d_* , as before. For a Froude number yielding unstable disturbances with intermediate wavelengths, $d_* \ll 1/k \ll d_+(T_*) \equiv (T_*/T_a)^\nu d_a < d_c$, all the approximations of Sec. V A are valid. Contrary to the two-length-scale model (47), the unperturbed solution for $T_a \ll T_* < T_c$, viewed at the length scale d_c , is not drastically different from the case with a continuous Spitzer conductivity. The analyses proceeds in three steps. The thermal equation (62) is first solved with the boundary conditions (15) at the critical surface. The solution is injected into Eq. (59) to obtain the kinematic relation, expressing m_a as a functional of the equation of the ablation surface, $x = \alpha_a(y, t)$. The flow is computed in terms of m_a by solving Eqs. (63) and (64) with the jump conditions (57), (58), and (60). The final result is given by the jump condition (61), in which the kinematic relation is injected.

VI. RESULTS FOR STRONGLY ACCELERATED FRONTS

Under ordinary conditions of implosion in ICF, the ablation front is submitted to strong accelerations such that both the marginal and the most linearly amplified disturbances have their wavelength ranging in the intermediate range $1/d_c \ll k \ll 1/d_*$.

A. Kinematic relation

The kinematic relation is obtained from Eqs. (57) and (59) when $\mathbf{n} \cdot \nabla T|_{x=\alpha_a}$ is expressed as a functional of $\alpha_a(y, t)$. It is instructive to consider the two models, (47) and (65), in parallel. The thermal equation (62) for the model (47) is linear. The solution $T_+ = \bar{T}_+ + \tilde{T}_+$ which verifies the boundary conditions at the critical surface, is, in the region where $\xi \ll -1/\hat{k}$, the same as in Eq. (52) where the first term in the right hand side is negligible

$$\tilde{T}_+(\xi) \approx -\frac{(T_c - T_a)}{2(d_c/d_a)} \sum \left[(e^{+i\hat{k} \cdot \eta + \hat{\sigma}\tau}) \frac{\hat{\alpha}_c}{d_a} e^{-\hat{k}\xi} \right], \quad (66)$$

with $\xi = (x - \alpha_c)/d_a$. The definition of the ablation front (53), yields the following relation, which may be used (at least in principle) to eliminate α_c in favor of α_a :

$$\begin{aligned} -\frac{(T_c - T_a)}{2(d_c/d_a)} \sum \left[(e^{+i\hat{k} \cdot \eta + \hat{\sigma}\tau}) \frac{\hat{\alpha}_c}{d_a} e^{-\hat{k}\alpha_a(\eta, \tau)/d_a} \right] \\ = \bar{T}_+(\xi = \bar{\alpha}_a/d_a) - \bar{T}_+(\xi = \alpha_a/d_a), \end{aligned} \quad (67)$$

where $\bar{\alpha}_c$ has been neglected in front of $\bar{\alpha}_a$ in the exponential on the left hand side and where $\bar{T}_+(\xi)$ is solution to $dT_+/d\xi - \lambda_+ d^2T_+/d\xi^2 = 0$. The solution is obtained in the same way with the model (65)

$$\tilde{Z}(\xi) \approx -\frac{(T_c - T_a)}{2} \sum \left[(e^{+i\hat{k} \cdot \eta + \hat{\sigma}\tau}) \frac{\hat{\alpha}_c}{d_a} e^{-\hat{k}\xi} \right], \quad (68)$$

with

$$\begin{aligned} -\frac{(T_c - T_a)}{2} \sum \left[(e^{+i\hat{k} \cdot \eta + \hat{\sigma}\tau}) \frac{\hat{\alpha}_c}{d_a} e^{-\hat{k}\alpha_a(\eta, \tau)/d_a} \right] \\ = \frac{\bar{T}_+^{\nu+1}(\xi = \bar{\alpha}_a/d_a)}{\nu+1} - \frac{\bar{T}_+^{\nu+1}(\xi = \alpha_a/d_a)}{\nu+1}. \end{aligned} \quad (69)$$

Taking the derivative of \tilde{Z} in Eq. (68), or of \tilde{T}_+ in Eq. (66), with respect to the normal coordinate, one gets

$$\begin{aligned} d_a \left(\lambda \mathbf{n} \cdot \nabla \frac{T_+}{T_a} \right) \Big|_{x=\alpha_a} \\ = \sqrt{1 + (\partial\alpha_a/\partial y)^2} \left(\frac{T_*}{T_a} - 1 \right) \left\{ 1 + \frac{(T_c - T_a)}{2(T_* - T_a)} \right. \\ \left. \times \sum \left[(e^{+i\hat{k} \cdot \eta + \hat{\sigma}\tau}) \hat{k} \frac{\hat{\alpha}_c}{d_a} e^{-\hat{k}\alpha_a(\eta, \tau)/d_a} \right] \right\}. \end{aligned}$$

The kinematic relation is obtained by eliminating $\hat{\alpha}_c(k)$ from this relation in favor of α_a with the help of Eqs. (67) or (69). The precise condition at the critical surface does not appear in the final result: In Eqs. (66) and (68), the quantity $(T_c$

$-T_a)\hat{\alpha}_c/2$ plays the same role as a constant of integration in the solution of Laplace equation (with a zero boundary condition at $\xi \rightarrow +\infty$) which is eliminated at the end in favor of α_a .

In the linear approximation, the term $e^{-\hat{k}\alpha_a(\eta, \tau)/d_a}$ on the left-hand side of Eqs. (67) and (69) is replaced by $e^{-\hat{k}\bar{\alpha}_a}$ which is no longer dependent on the transverse variable η , while the right-hand side is proportional to $\bar{\alpha}_a/d_a = \Sigma[(e^{+i\hat{k} \cdot \eta + \hat{\sigma}\tau}) \hat{\alpha}_c/d_a]$. For the model (47), this leads to Eq. (54) with the same relation between $\hat{\alpha}_c(k)$ and $\hat{\alpha}_a(k)$ as in Sec. IV B, while $\delta\tilde{Z}$ of the model (65) is given by Eq. (54) multiplied by $(T_*/T_a)^\nu$. Both models yield the same linear approximation of the right-hand side of Eq. (59)

$$\begin{aligned} d_a \delta[(\lambda \mathbf{n} \cdot \nabla T_+)|_{x=\alpha_a}] \\ = \left(\frac{T_*}{T_a} - 1 \right) \sum \left[(e^{+i\hat{k} \cdot \eta + \hat{\sigma}\tau}) \hat{k} \frac{\hat{\alpha}_a}{d_a} \right], \end{aligned} \quad (70)$$

and the same linear kinematic relation

$$\tilde{u}_{a-} - \partial\tilde{\alpha}_a/\partial t = V_a K(\tilde{\alpha}_a), \quad (71)$$

obtained from Eqs. (59) and (70) with, according to Eq. (57), $\tilde{m}_a = (\tilde{u}_{a-} - \partial\alpha_a/\partial t)/V_a$, and where $K(\cdot)$ is a pseudo-differential operator defined in the Fourier space as the multiplication by the modulus of wave vector k

$$K(\tilde{\alpha}) = \sum_{\kappa' > 0} \kappa' \hat{\alpha}(\kappa') e^{i\kappa' \eta} - \sum_{\kappa' < 0} \kappa' \hat{\alpha}(\kappa') e^{i\kappa' \eta}. \quad (72)$$

Equation (71) means that the ablation front is convected by the upstream flow with a relaxation mechanism similar to Eq. (10). This relation depends neither on the precise definition of the ablation front nor on the model for the thermal conductivity, and is valid for $kd \gg 1$, irrespective of the values of T_* and ν , provided that $T_c > T_* \gg T_a$ and $d_-(T_*) \ll d_+(T_*)$.

The result takes a more complicated form in the nonlinear case. The elimination of $\hat{\alpha}_c(k)$ may be obtained order by order. The result is still independent of the model when the nonlinear terms on the right hand side of Eqs. (67) and (69) are neglected in front of the nonlinear terms on the left hand side, as it is consistent with the basic assumption of the model, $(T_a/T_*)^\nu \ll kd_a \equiv \hat{k} \ll 1$, see the discussion below Eq. (65). In the quadratic approximation, the kinematic relation takes the form

$$\begin{aligned} \frac{(u_{a-} - \partial\alpha_a/\partial t - v_{a-} \partial\alpha_a/\partial y)}{V_a} \\ = 1 + K(\tilde{\alpha}_a) + K[\tilde{\alpha}_a K(\tilde{\alpha}_a)] + \frac{\partial}{\partial y} \left[\tilde{\alpha}_a \frac{\partial}{\partial y} \tilde{\alpha}_a \right]. \end{aligned} \quad (73)$$

However, the linearization on the right hand side of Eqs. (67) and (69) clearly limits the amplitude of the corrugations of the ablation front to values smaller than $d_+(T_*)$. For describing accurately large amplitudes it would be better to follow the same strategy, but without linearization on the right-hand side.

B. Linear analysis

Once the kinematical relation (71) is known, the linear dynamics of the ablation front is obtained by solving the linearized version of the incompressible Euler equations (63) and (64) with the jump conditions across the ablation front (57) and (58) and (60) and (61). Using the same nondimensional variables as in Eqs. (25)–(28), but now with $\alpha \rightarrow \alpha_a$ and $\xi \rightarrow \zeta$

$$\tilde{X}(\zeta, \eta, \tau) = \sum \hat{X}(\zeta) (\hat{\alpha}_a / d_a) e^{\pm i k \eta + \hat{\sigma} \tau},$$

$$\zeta \equiv (x - \alpha_a) / d_a,$$

the nondimensional jump conditions may be expressed in the linear approximation in term of the perturbation of the mass flux across the ablation front, $\hat{m}_a \equiv \hat{u}_-(\zeta=0) - \hat{\sigma}$, see Eq. (57), as

$$\zeta = 0: \quad \hat{u}_+ = a_* \hat{m}_a + \hat{\sigma}, \quad \hat{u}_- = \hat{m}_a + \hat{\sigma}, \quad (74)$$

$$\hat{v}_+ - \hat{v}_- = -i \hat{k} (a_* - 1) \approx -i \hat{k} a_*, \quad (75)$$

$$\begin{aligned} \hat{\pi}_+ - \hat{\pi}_- &= -2(a_* - 1) \hat{m}_a + (1 - a_*^{-1}) Fr^{-1}, \\ &\approx -2a_* \hat{m}_a + Fr^{-1}, \end{aligned} \quad (76)$$

where $\pi \equiv p - \rho g x / V_a^2$, and

$$a_* \equiv \rho_a / \rho_* \gg 1, \quad Fr^{-1} \equiv g d_a / V_a^2. \quad (77)$$

The linear kinematic relation (71) takes the form,

$$\hat{m}_a = \hat{k}. \quad (78)$$

Ablation fronts in ICF, or RT interfaces, differ from flames by the form of the kinematic relation. One has $\hat{m}_a = 0$ for the analysis of DL-instability, and $\hat{m}_a \propto (d_c k) \hat{k}$ when the curvature effects are taken into account in flame theory. However, in this last case, additional curvature terms¹⁶ must be introduced in the jump conditions (74)–(76) to recover the same coefficient in front of $d_c k$ in Eq. (8). For improving the physical insights, it is convenient to carry out the linear analysis in term of \hat{m}_a , introducing the kinematic relation, i.e., the expression $\hat{m}_a(\hat{k})$, at the end of the calculation.

For unstable situations, $\text{Re } \hat{\sigma} > 0$, the linear solutions of Eqs. (63) and (64) that are decreasing to zero for $\zeta \rightarrow -\infty$ (cold side) and for $\zeta \rightarrow +\infty$ (hot side) are

$$\hat{u}_- = U_- e^{+k \zeta}, \quad \hat{v}_- = i \hat{u}_-, \quad (79)$$

$$\hat{\pi}_- = -(\hat{\sigma} + \hat{k}) U_- e^{+k \zeta} / \hat{k}, \quad (80)$$

$$\hat{u}_+ = U_p e^{-k \zeta} + U_r e^{-\hat{\sigma} \zeta / a_*}, \quad i \hat{k} \hat{v}_+ = -\partial \hat{u}_+ / \partial \zeta, \quad (81)$$

$$\hat{\pi}_+ = (\hat{\sigma} - a_* \hat{k}) U_p e^{-k \zeta} / a_* \hat{k}, \quad (82)$$

where the unknown constants of integration, U_- , U_p , and U_r are the amplitude of the perturbed flow in the cold medium and of the potential and rotational part of the perturbed flow in the downstream region. These coefficients may be expressed in term of \hat{m}_a by using Eqs. (74) and (75)

$$U_- = \hat{m}_a + \hat{\sigma}, \quad (83)$$

$$\begin{aligned} U_r \left(1 - \frac{\hat{\sigma}}{a_* \hat{k}} \right) &= (a_* + 1) \hat{m}_a + 2 \hat{\sigma} - (a_* - 1) \hat{k}, \\ &\approx a_* \hat{m}_a + 2 \hat{\sigma} - a_* \hat{k}, \end{aligned} \quad (84)$$

$$\begin{aligned} U_p \left(1 - \frac{\hat{\sigma}}{a_* \hat{k}} \right) &= (a_* - 1) \hat{k} - \left(1 + \frac{\hat{\sigma}}{\hat{k}} \right) \hat{m}_a - \left(1 + \frac{\hat{\sigma}}{a_* \hat{k}} \right) \hat{\sigma}, \\ &\approx a_* \hat{k} - \left(1 + \frac{\hat{\sigma}}{\hat{k}} \right) \hat{m}_a - \left(1 + \frac{\hat{\sigma}}{a_* \hat{k}} \right) \hat{\sigma}. \end{aligned} \quad (85)$$

The pressure jump in Eq. (76) with Eqs. (80), (82), (83), and (85) then leads to a quadratic equation for $\hat{\sigma}$

$$\begin{aligned} \hat{\sigma}^2 \left(1 + \frac{1}{a_*} \right) + 2(\hat{m}_a + \hat{k}) \hat{\sigma} - \left[\left(1 - \frac{1}{a_*} \right) Fr^{-1} \hat{k} \right. \\ \left. + (a_* - 1) \hat{k}^2 - 2a_* \hat{m}_a \hat{k} \right] &= 0, \end{aligned} \quad (86)$$

yielding at the leading order in the limit $a_* \gg 1$

$$\hat{\sigma}^2 + 2(\hat{m}_a + \hat{k}) \hat{\sigma} - [Fr^{-1} \hat{k} + a_* \hat{k}^2 - 2a_* \hat{m}_a \hat{k}] \approx 0. \quad (87)$$

C. Discussion of the linear stability and comparison with flames

The marginally stable wave number, separating unstable and stable ranges, is given by the zero of the bracket in Eq. (87). The first and second term represent the RT and DL instability, respectively, while the third one describes the stabilization due to thermal conduction. It is worth noticing the origin of these terms. Each term in the bracket comes from the pressure jump (76) multiplied by \hat{k} : The RT term, $Fr^{-1} \hat{k}$, and the kinematic one, $-2a_* \hat{m}_a \hat{k}$, both come from the right-hand side of Eq. (76), while the DL term, $a_* \hat{k}^2$, comes from the expression of $\hat{\pi}_+$ in the left hand side, computed with the potential part of the flow downstream the ablation front, see Eq. (82) with the first term on the right-hand side of Eq. (85).

The case for flames, see Eqs. (5) and (7), is recovered by setting $a_* = a \equiv \rho_a / \rho_c$, replacing d_a by d_c (i.e., Fr^{-1} by $a^\nu Fr^{-1}$, \hat{k} and $\hat{\sigma}$ by $k d_c$ and $\sigma d_c / V_a$, respectively), and by using a kinematic relation of the form, $\hat{m}_a = 0$ for the DL analysis, or $\hat{m}_a \propto (d_c k) \hat{k}$ to take into account the modifications to the flame structure by wrinkling. Coming back to strongly accelerated ablation front in ICF, the two last terms inside the bracket [] of Eq. (87) make clear how the DL instability is damped out by the kinematic relation (78), $\hat{m}_a = \hat{k} \Rightarrow a_* \hat{k}^2 - 2a_* \hat{m}_a \hat{k} = -a_* \hat{k}$, leading to

$$\hat{\sigma}^2 + 4\hat{k} \hat{\sigma} - \hat{k} [Fr^{-1} - a_* \hat{k}] \approx 0, \quad (88)$$

yielding in the limit $a_* \gg 1$

$$\hat{\sigma} \approx \sqrt{Fr^{-1} \hat{k} - a_* \hat{k}^2} - 2\hat{k}, \quad (89)$$

where the term of following order, $-2\hat{k}$, is useful in the stable domain. The orders of magnitude of the cut-off wave number, of the most amplified wave number and of the maximum linear growth rate are

$$\hat{k} \equiv kd_a = O(Fr^{-1}/a_*), \quad \hat{\sigma} \equiv \sigma d_a/V_a = O(Fr^{-1}/\sqrt{a_*}), \quad (90)$$

showing that the validity of Eqs. (86)–(89) in the full unstable range is limited to accelerations corresponding to intermediate Froude numbers

$$1/d_c \ll k \ll 1/d_a \Rightarrow a_* / a^v \ll Fr^{-1} \ll a_*. \quad (91)$$

According to Eq. (90), one has $\hat{\sigma}/\hat{k} \gg 1$ and $\hat{\sigma}/a_* \hat{k} \ll 1$,

$$\hat{\sigma}/\hat{k} = O(\sqrt{a_*}), \quad \hat{\sigma}/a_* \hat{k} = (1/\sqrt{a_*}), \quad (92)$$

and, according to Eqs. (78)–(85), the order of magnitude of the flow is

$$\hat{u}_- \approx \hat{\sigma} e^{+\hat{k}\xi} = O(Fr^{-1}/\sqrt{a_*}), \quad (93)$$

$$\hat{p}_- \approx -(\hat{\sigma}^2/\hat{k}) e^{+\hat{k}\xi} = O(Fr^{-1}), \quad (94)$$

$$\hat{u}_{p+} \approx a_* \hat{k} e^{-\hat{k}\xi} = O(Fr^{-1}), \quad (95)$$

$$\hat{u}_{r+} \approx 2\hat{\sigma} e^{-\hat{\sigma}\xi/a_*} = O(Fr^{-1}/\sqrt{a_*}), \quad (96)$$

$$\hat{p}_+ \approx -a_* \hat{k} e^{-\hat{k}\xi} = O(Fr^{-1}). \quad (97)$$

According to Eqs. (84) and (85), the kinematic relation (78) makes the rotational part of the flow smaller than its potential part, see the ordering (95) and (96). In the limit of a large density jump across the ablation front, the leading order of the flow in the hot side (downstream the ablation front) is potential and quasi-steady, see Eqs. (95) and (97).

Equation (86) with (78), and Eq. (89) are in agreement with the results of the two-length-scale model⁹ (47) and of the SBL.^{8,11} The problem left for a comparison with the model of a continuous conductivity Spitzer is the determination of the coefficient a_* , controlling the density jump across the ablation front, see Eqs. (74)–(77). Although the kinematic relation is independent of T_* , the final result depends on ρ_* through the perturbed flow. By construction, T_* must correspond to an intermediate length scale $d(T)$ of the continuous model, between $kd(T) \ll 1$ and $kd(T) \gg 1$, and the natural choice for T_* is then $kd(T_*) \approx 1$, $\hat{k} \approx (T_*/T_a)^v$, leading to the coefficient a_* depending on the wave number, $a_* \approx (1/\hat{k})^{1/v}$. In fact, the result of Goncharov *et al.*³ which leads to an accurate dispersion relation by comparison with the numerical results, corresponds more precisely to Eq. (86) with $a_* = (\nu/\hat{k})^{1/v}$. The coefficient ν in this expression may be anticipated from Eq. (20), where the reduced length scale appears to be more precisely \bar{T}^ν/ν .

D. Tests of consistency

To conclude this section it is worth coming back briefly to approximations (62)–(64) in Sec. V A, for checking their validity on the final result. According to Eqs. (13) and (28), the flow introduces additional terms in Eq. (62), yielding in the linear and quasi-steady state approximations

$$\frac{d\hat{T}_+}{d\xi'} - \left(\frac{d^2}{d\xi'^2} - \hat{k}^2 \right) \bar{T}^\nu \hat{T}_+ = (\hat{T}_+ - \hat{u}_+) \frac{1}{\bar{T}} \frac{d\bar{T}}{d\xi'}, \quad (98)$$

where the relation $\hat{m}_\alpha \approx (\hat{u}_+ - \hat{T}_+)/\bar{T}$ has been used. The order of magnitude of the terms on the right-hand side of Eq.

(98), may be evaluated with the leading order solution, written in the notations of Secs. VIB and VIC as $\bar{T}^\nu \hat{T}_+ \approx -a_* e^{-\hat{k}\xi}$, see Eq. (54), and $\hat{u}_+ \approx a_* \hat{k} e^{-\hat{k}\xi}$, see Eq. (95). By using Eq. (18), $\bar{T}^\nu d\bar{T}/d\xi' \approx \bar{T}$, the last term on the right-hand side is found to be of same order as the first term in the left-hand side, both smaller than the last term on the left-hand side by a factor $1/kd$, with $kd = \hat{k}\bar{T}^\nu \gg 1$. The first term on the right-hand side is even smaller, showing that the density perturbation is negligible in the leading order of the mass flux, $\bar{T}\hat{m}_\alpha \approx \hat{u}_+$. In the same approximation as for Eq. (98), the Euler equations (25), (26), and (27) lead to

$$\frac{d}{d\xi'} (\bar{T}\hat{m}_\alpha) - \frac{1}{\hat{k}^2} \frac{d^2}{d\xi'^2} \left(\bar{T} \frac{d}{d\xi'} \hat{m}_\alpha \right) = - \frac{d}{d\xi'} \hat{T}_+ - \hat{m}_\alpha \frac{d\bar{T}}{d\xi'}, \quad (99)$$

where the two terms on the right-hand side are introduced in the Euler equations by the density variation and are of the same order of magnitude, $a_* \hat{k}/\bar{T}^\nu$. They are both smaller by a factor $1/kd$ than the terms on the left hand side, where the spatial dependence of \bar{T} introduces also small terms of relative order $1/kd$. This confirms that the flow downstream of the ablation front is incompressible in first approximation.

VII. WEAKLY NONLINEAR ANALYSIS

The method presented in Sec. V is convenient for a nonlinear study, devoted to derive a pseudo-differential equation for the evolution of the ablation front, irrespective of the number of unstable modes. In view of studying nonlinear transfers occurring at the beginning of the period of strong acceleration, see the last paragraph of the introduction, we carry out a weakly nonlinear analysis, limited to quadratic order of an expansion in gradient intensity, using $k\tilde{\alpha}_a \ll 1$ as a small parameter. A simplification appears for a large density jump, $a_* \gg 1$: According to Eqs. (92), (95), and (96), the rotational part of the flow downstream from the ablation front, becomes negligible in front of its potential part. In this case, the rotational term $\tilde{\mathbf{v}} \times (\nabla \times \tilde{\mathbf{v}})$ is negligible in front of the gradient of kinetic energy, $\nabla(\tilde{v}^2/2)$ and, according to Eqs. (11) and (12), the flow satisfies the Bernoulli equation

$$\left(\frac{\partial}{\partial \tau} + \bar{u}_\pm \frac{\partial}{\partial \xi} \right) \mathbf{v}_\pm \approx \mathbf{g} - \nabla \left(\frac{p_\pm}{\bar{\rho}_\pm} + \frac{1}{2} \tilde{v}_\pm^2 \right), \quad \nabla \cdot \tilde{\mathbf{v}}_\pm = 0.$$

Using a Fourier representation for the disturbances when wrinkling the front (the unperturbed front is planar), the flow may be expressed in terms of three quantities U_- , U_r , U_p , as in Eqs. (79)–(82), with notations similar to Secs. VIB and VIC, but now where ξ is replaced by $\xi' \equiv x/d_a$ and

$$\pi_\pm \equiv p_\pm + \bar{\rho}_\pm \tilde{v}_\pm^2/2 - \bar{\rho}_\pm g x/V_a^2,$$

written with nondimensional variables ($\mathbf{v}/V_a \rightarrow \mathbf{v}$, $p/\rho_a V_a^2 \rightarrow p$, $\bar{\rho}_- = 1/\bar{u}_- = 1$, $\bar{\rho}_+ = 1/\bar{u}_+ = 1/a_*$). The values of the flow (and its derivative) at the ablation front is given when ξ is replaced by $\alpha_a(\eta, \tau)/d_a$, yielding, for example,

$$\tilde{u}_{a-} = \sum [(e^{+ik \cdot \eta + \hat{\sigma}\tau})e^{+k\alpha_a(\eta, \tau)/d_a} U_-], \quad (100)$$

to give, at the first order of a gradient expansion

$$\tilde{u}_{a-} = \tilde{u}_-|_{x=\bar{\alpha}_a} + \tilde{\alpha}_a(\eta, \tau)K(\tilde{u}_-|_{x=\bar{\alpha}_a}) + \dots, \quad (101)$$

where the pseudo-differential operator $K(\cdot)$ is defined in Eq. (72), and where

$$\tilde{u}_-|_{x=\bar{\alpha}_a} \equiv \sum [(e^{+ik \cdot \eta + \hat{\sigma}\tau})e^{+k\bar{\alpha}_a/d_a} U_-]. \quad (102)$$

The other components of the flow and the pressure may be expressed in the same way. For example, $\tilde{v}_-(\xi', \eta, \tau) = H(\tilde{u}_-)$, where $H(\cdot)$ is the Hilbert operator

$$H(\tilde{u}_-) = \sum_{\kappa' > 0} i\hat{a}(\kappa')e^{i\kappa'\eta} - \sum_{\kappa' < 0} i\hat{a}(\kappa')e^{i\kappa'\eta}, \quad (103)$$

and the gradient expansion yields

$$\tilde{v}_{a-} = H(\tilde{u}_-|_{x=\bar{\alpha}_a}) + \tilde{\alpha}_a(\eta, \tau)\partial(\tilde{u}_-|_{x=\bar{\alpha}_a})/\partial\eta + \dots \quad (104)$$

The computation is carried out in a way quite similar to Sec. VI B. The quantities U_- , U_r , and U_p are expressed in terms of m_a by using the boundary conditions in Eqs. (57), (58), and (60). A pseudo-differential equation for the evolution of the ablation front is then obtained by using the boundary condition (61) in which the kinematic relation (73) is introduced. Introducing nondimensional variables, coming from the scalings in Eq. (90), $X \equiv \xi' Fr^{-1}/a_*$, $Y \equiv \eta Fr^{-1}/a_*$, $\mathcal{T} \equiv \tau Fr^{-1}/\sqrt{a_*}$ and $A \equiv (\alpha_a/d_a) Fr^{-1}/a_*$, the equation for the evolution of the ablation front, $X = A(Y, \mathcal{T})$, takes the following form, free from parameters (the small parameter ϵ excepted)

$$\begin{aligned} \partial^2 A / \partial \mathcal{T}^2 - \partial^2 A / \partial Y^2 - K(A) + \epsilon K(\partial A / \partial \mathcal{T}) \\ = \partial^2 B / \partial Y^2 + \partial C / \partial Y - K(D), \end{aligned} \quad (105)$$

where

$$\begin{aligned} B &\equiv AK(A), \\ C &\equiv -AA'_Y + AK(A'_Y) - \dot{A}_\mathcal{T}H(\dot{A}_\mathcal{T}), \\ D &\equiv AK(A) + 2AA''_{YY} + A_Y'^2/2 + [K(A)]^2/2 + \dot{A}_\mathcal{T}^2/2 \\ &\quad + [H(\dot{A}_\mathcal{T})]^2/2, \end{aligned}$$

and where the notations $A'_Y \equiv \partial A / \partial Y$, $\dot{A}_\mathcal{T} \equiv \partial A / \partial \mathcal{T}$ have been used. The left-hand side of Eq. (105) corresponds to the dispersion relation (88). The parameter $\epsilon \equiv 4/\sqrt{a_*}$ is small in the limit $a_* \gg 1$, and the last term of following order in the left-hand side of Eq. (105), $\epsilon K(\partial A / \partial \mathcal{T})$, represents the leading order damping rate in the stable domain ($K > 1$). Numerical solution to Eq. (105) with an initial condition given by the end of the first period of irradiation (when the acceleration was negligible) describes the development of the nonlinear structures, at the beginning of the accelerated phase. Detailed results will be presented in a forthcoming paper. A first insight into the nonlinear transfer mentioned at the end of the introduction is provided in a simple case, when attention is

limited to only two unstable modes, $A = A_1(\mathcal{T}) \exp(iKY) + A_2(\mathcal{T}) \exp(2iKY) + cc$. In this case, Eq. (105) reduces to

$$\begin{aligned} \frac{d\dot{A}_{1\mathcal{T}}}{d\mathcal{T}} - (K - K^2)A_1 &= -2K\dot{A}_{2\mathcal{T}}\dot{A}_{1\mathcal{T}}^* - 2K^2A_2A_1^*, \\ \frac{d\dot{A}_{2\mathcal{T}}}{d\mathcal{T}} - 2(K - 2K^2)A_2 &= +2K\dot{A}_{1\mathcal{T}}^2 - 2K^3A_1^2, \end{aligned}$$

in agreement with recent mode-mode coupling analyses.^{12,17} The transfer from the first to the second mode is represented by the solution corresponding to an initial condition for which only the amplitude of the first mode is nonzero, $\mathcal{T} = 0: A_2 = 0, A_1 = A_{1i} \neq 0$. This solution shows that the second mode grows with an amplitude proportional to $K|A_{1i}|^2$, to be compared with the linear result where the amplitude of the second mode at the end of the first period of irradiation (g negligible), $|A_{2i}|$, may be much smaller than $K|A_{1i}|^2$. Equation (105) is more general and not limited to a small number of modes. This equation is able to describe a continuous cascade for feeding the short wavelength modes that are the most amplified during implosion (strong acceleration), with the large wavelength modes that were amplified by the DL instability during the first period of irradiation (weak acceleration).

VIII. CONCLUDING REMARKS

A first outcome of the present analysis is to describe how, and in what conditions, the DL instability may be dominated by thermal relaxation in strongly RT unstable flames or ablation fronts. When the heat conductivity varies strongly across the wave structure, a transition in the linear dynamics of the wave is seen to occur with increasing the RT instability, see Fig. 3, filling the gap between flames propagating upwards and strongly accelerated ablation fronts in ICF. This result is useful, not only from a fundamental point of view, but also for describing the early development of nonlinear structures on the ablation front in ICF. When attention is focused on relaxation of disturbances with intermediate wavelengths, shorter than the thermal-diffusion lengths downstream of the ablation front, but larger than the thickness of this front, a noteworthy property (resulting from separation of scales) is pointed out: The kinematic relation for the local dynamics of the ablation front is independent of the details of the model. In the linear approximation, this relation takes a simple form, see Eq. (71), leading to an anti-DL damping rate at small wavelengths. A weakly nonlinear pseudo-differential equation for the evolution of the ablation front in ICF is also derived for studying the development of nonlinear structures, irrespective of the number of unstable modes. Although its validity is limited in time, this equation is useful, especially when the length of time of the acceleration period, prior to ignition, is not much larger than the inverse of the growth rate of the most amplified disturbance. Another concern is the influence of the first period of irradiation, when the acceleration of the front is not yet strong. The development of initial disturbances during this first period, subjected to a DL instability at large wavelengths (larger than d_c or of same order) and to strong stabi-

lization at small wavelengths (smaller than d_c), must play a non negligible role in the final amplitude (prior to ignition) of the nonlinear structures whose size is much smaller than d_c . A nonlinear transfer through a cascade for feeding the small-scale structures may be analyzed numerically with the weakly nonlinear equation derived in this paper. An extension of this work will be carried out in spherical geometry, concerning the shrinking of wavelengths with decreasing radius of the shell during implosion.

ACKNOWLEDGMENTS

We wish to thank Professor Y. Pomeau, Professor J. Sanz, and Professor F. A. Williams for fruitful discussions.

The research was supported in part by the CEA/DAM through Grant No. 4600051147/P6H29 and by Institut Universitaire de France.

¹J. Lindl, Phys. Plasmas **2**, 3933 (1995).

²S. Bodner, Phys. Rev. Lett. **33**, 761 (1974).

³V. Goncharov, R. Betti, R. L. McCrory, P. Sorotokin, and C. P. Verdon, Phys. Plasmas **3**, 1402 (1996).

⁴J. Sanz, Phys. Rev. Lett. **73**, 2700 (1994).

⁵H. Takabe, L. Monthieth, and R. Morse, Phys. Fluids **26**, 2299 (1983).

⁶H. Takabe, K. Mima, L. Monthieth, and R. Morse, Phys. Fluids **28**, 3676 (1985).

⁷H. J. Kull, Phys. Fluids B **1**, 170 (1989).

⁸A. Piriz, J. Sanz, and L. Ibáñez, Phys. Plasmas **4**, 1117 (1997).

⁹L. Masse, Ph.D. thesis, Université de Provence (2001).

¹⁰V. Goncharov, Phys. Rev. Lett. **82**, 2091 (1999).

¹¹A. Piriz, Phys. Plasmas **8**, 997 (2001).

¹²J. Sanz, J. Ramírez, R. Ramis, R. Betti, and R. P. J. Town, Phys. Rev. Lett. **89**, 195002 (2002).

¹³P. Clavin, Prog. Energy Combust. Sci. **11**, 1 (1985).

¹⁴P. Clavin, Annu. Rev. Fluid Mech. **26**, 321 (1994).

¹⁵P. Clavin, in *Proceedings of the Combustion Institute* (The Combustion Institute, Pittsburgh, 2000), Vol. 28, pp. 569–586.

¹⁶P. Clavin and P. Garcia, J. Mec. Theor. Appl. **2**, 245 (1983).

¹⁷J. Garnier, P. Raviart, C. Cherfils-Clerouin, and L. Masse, Phys. Rev. Lett. **90**, 185003 (2003).

¹⁸G. I. Sivashinsky, Acta Astronaut. **4**, 1177 (1977).

¹⁹P. Clavin and B. Denet, Phys. Rev. Lett. **88**, 044502 (2002).

²⁰G. I. Sivashinsky and P. Clavin, J. Physique **48**, 193 (1987).

²¹P. Clavin and F. Williams, J. Fluid Mech. **116**, 251 (1982).

²²P. Pelcé and P. Clavin, J. Fluid Mech. **124**, 219 (1982).

²³M. Matalon and B. Matkowsky, J. Fluid Mech. **116**, 239 (1982).

²⁴P. Clavin and G. Joulin, J. Phys. B **1**, 1 (1983).